



# Modelling emission and transport of key components of primary marine organic aerosol using the global aerosol–climate model ECHAM6.3–HAM2.3

Anisbel Leon-Marcos<sup>1</sup>, Moritz Zeising<sup>2</sup>, Manuela van Pinxteren<sup>3</sup>, Sebastian Zeppenfeld<sup>3</sup>, Astrid Bracher<sup>2,4</sup>, Elena Barbaro<sup>5</sup>, Anja Engel<sup>6</sup>, Matteo Feltracco<sup>7</sup>, Ina Tegen<sup>1</sup>, and Bernd Heinold<sup>1</sup>

<sup>1</sup>Modelling of Atmospheric Processes Department, Leibniz Institute for Tropospheric Research, Leipzig, Germany

<sup>2</sup>Climate Science Department, Alfred Wegener Institute, Helmholtz Centre for Polar and Marine Research, Bremerhaven, Germany

<sup>3</sup>Atmospheric Chemistry Department (ACD), Leibniz Institute for Tropospheric Research, Leipzig, Germany

<sup>4</sup>Institute of Environmental Physics, University of Bremen, Bremen, Germany

<sup>5</sup>Institute of Polar Sciences – CNR, Venice, Italy

<sup>6</sup>Marine Biogeochemistry Department, GEOMAR Helmholtz Centre for Ocean Research, Kiel, Germany

<sup>7</sup>Department of Environmental Sciences, Informatics and Statistics, CaFoscari University of Venice, Venice Mestre, VE, Italy

**Correspondence:** Bernd Heinold (heinold@tropos.de)

Received: 18 September 2024 – Discussion started: 30 September 2024

Revised: 7 February 2025 – Accepted: 2 April 2025 – Published: 10 July 2025

**Abstract.** Primary marine organic aerosol (PMOA) contributes significantly to the aerosol loading over remote oceanic regions, where sea spray dominates aerosol production in the lower troposphere, and plays an important role in aerosol–cloud–climate interactions. The sea–atmosphere transfer of organic components depends on their abundance at the ocean surface and their physicochemical characteristics. We introduce a novel approach for representing the ocean concentration of the most abundant organic groups in seawater that are relevant for aerosols. By apportioning the phytoplankton-exuded dissolved organic carbon, modelled in the biogeochemistry model FESOM2.1–REcoM3, three biomolecule groups are computed (dissolved carboxylic acidic containing polysaccharides (PCHO), dissolved combined amino acids (DCAA), and polar lipids (PL)). The transfer of these marine groups to the atmosphere is represented by the OCEANFILMS (Organic Compounds from Ecosystems to Aerosols: Natural Films and Interfaces via Langmuir Molecular Surfactants) parameterization which is implemented in the aerosol–climate model ECHAM6.3–HAM2.3 to represent the emission and transport processes in the atmosphere. The concentration of biomolecules in the ocean serves as the bottom boundary condition for the PMOA simulation within the aerosol model. Among the sim-

ulated organic groups in seawater, modelled PCHO is the most prevalent, followed by DCAA and PL. Conversely, PL contributes the most to the organic matter in aerosols, given the high air–seawater affinity of lipids compared to the other groups. Biomolecules exhibit minor variations in equatorial waters, whereas strong seasonal patterns are observed towards the polar regions. The global aerosol model simulations indicate that PMOA emission fluxes are primarily influenced by marine biological activity and surface wind conditions. Based on the most comprehensive evaluation to date, the computed levels of biomolecules in the ocean and species-resolved PMOA concentrations are compared with ground-based measurements across the globe. The comparison shows a reasonably good agreement, given the uncertainties in model assumptions and measurements. Model biases in the representation of the marine organic aerosol groups are caused by uncertainties in the aerosol-process representation and the simulated sea salt concentrations. A comparison with a set of long-range in situ aircraft measurements indicates that by including PMOA in the model, the representation of organic aerosols in the southern oceans is significantly improved.

## 1 Introduction

Oceans are a major source of natural aerosols (O'Dowd et al., 1997; Simó, 2004; Lewis and Schwartz, 2004; Galí et al., 2018; Rinaldi et al., 2020). Wind-generated sea spray aerosol (SSA) particles predominate in the marine boundary layer (Blanchard and Woodcock, 1980; O'Dowd et al., 1997; Lewis and Schwartz, 2004). They therefore significantly influence the climate system through aerosol–radiation and aerosol–cloud interactions in remote marine and coastal regions (Pandis et al., 1994; Murphy et al., 1998; Carlsaw et al., 2013; Vergara-Temprado et al., 2017).

Multiple experimental studies simulating air bubble bursting have demonstrated that marine organic constituents are co-emitted with sea salt in sea spray (Keene et al., 2007; Facchini et al., 2008; Schmitt-Kopplin et al., 2012). This so-called primary marine organic aerosol (PMOA) emitted directly this way dominates the sub-micron range of the sea spray particle size distribution (Facchini et al., 2008; Gantt et al., 2011; Gantt and Meskhidze, 2013). Nonetheless, organics also contribute to the chemical composition of the coarse mode of sea salt aerosol particles (Hawkins and Russell, 2010; Russell et al., 2010; Leck et al., 2013; Zeppenfeld et al., 2021).

Many organic compounds detected in ambient marine samples are found to be highly enriched in the surface microlayer (SML) with respect to bulk water (Engel et al., 2017; Pinxteren et al., 2017; Triesch et al., 2021a, b; Zeppenfeld et al., 2023). The SML is the uppermost layer of the ocean, which often contains high concentrations of organic compounds that cover the surface of rising bubbles before bursting (Stefan and Szeri, 1999; Sellegri et al., 2006; Bigg and Leck, 2008). The characterized fraction of organic matter in the ocean is dominated by lipid-like, polysaccharidic and proteinaceous compounds (Wakeham et al., 1997; Repeta, 2015) that have also been detected inside aerosol particles (Frossard et al., 2014; van Pinxteren et al., 2023). The formation of PMOA is determined by the physicochemical properties of marine organic compounds, with the transfer from bulk water to SML to the atmosphere occurring in a chemo-selective manner (Facchini et al., 2008; Schmitt-Kopplin et al., 2012; Burrows et al., 2014). Highly surface-active molecules are preferably transferred compared to non-surface-active constituents. Thus, a differential enrichment is found in the aerosols compared to their analogues in seawater (Rastelli et al., 2017; van Pinxteren et al., 2023).

For a long time, there has been a high level of interest in the modelling of the emission, transport and physicochemical properties of PMOA in the context of aerosol–climate studies (O'Dowd et al., 2008; Vignati et al., 2010; Long et al., 2011; Albert et al., 2012; Gantt et al., 2012a; Vergara-Temprado et al., 2017). Various parametrizations, based on chlorophyll-*a* (chl-*a*) ocean concentration as a proxy for marine biological activity, have been used to account for wind-driven emissions of PMOA (O'Dowd et al., 2008; Gantt et al., 2011;

Long et al., 2011; Rinaldi et al., 2013). Nevertheless, chl-*a* does not correlate with the organic fractions in aerosol particles in some regions (Prather et al., 2013; Collins et al., 2016), especially in oligotrophic waters. Hence, a more physically based framework to parameterize the coverage of surfactants on the bubble film and the relative enrichment in the aerosols was introduced by Burrows et al. (2014). The scheme requires input data that account for the presence of the most abundant macromolecules in the ocean. To this end, an ocean biogeochemistry model is needed to compute these quantities (Burrows et al., 2014; Ogunro et al., 2015).

Both methods of estimating PMOA mass fractions have been included and validated in global models (Meskhidze et al., 2011; Gantt et al., 2012b; Gantt and Meskhidze, 2013; Huang et al., 2018; Han et al., 2019). Recently, Zhao et al. (2021) found that the scheme by Burrows et al. (2014) yields an improvement in the representation of PMOA compared to a chl-*a*-based approach. Some modelling studies have additionally implemented the ability of PMOA to serve as ice nucleating particles (INPs) based on empirical formulations (Wilson et al., 2015; DeMott et al., 2016; McCluskey et al., 2018b). Special attention has been given to the significance of PMOA in the climate system as relevant INPs and, to a lesser extent, as cloud condensation nuclei (CCN), especially over remote marine environments (Gantt et al., 2012b; Burrows et al., 2013; Yun and Penner, 2013; Huang et al., 2018; Vergara-Temprado et al., 2018; Zhao et al., 2021; Burrows et al., 2022). The characteristics of the chemical compounds are also assumed to be important for their ice formation potential. There is evidence of high ice activity for marine polysaccharidic and proteinaceous compounds compared to other measured organic groups (McCluskey et al., 2018a; Alpert et al., 2022). Thus, representing PMOA as an independent component is crucial to establishing a solid foundation for future research on the climate impact of these biological compounds, particularly their effects on mixed-phase clouds.

To further investigate the occurrence of different PMOA species in various climate regions, we implement the sophisticated PMOA emission scheme by Burrows et al. (2014) in the global aerosol–climate model ECHAM6.3–HAM2.3 (Tegen et al., 2019). With regard to the marine boundary conditions, an approach for calculating the most important organic compounds in the ocean is introduced. In this approach, the contribution to the dissolved organic carbon (DOC) from the phytoplankton exudation is considered in contrast to carbon release via cell lysis by Burrows et al. (2014). The approach is based on simulation results from the detailed marine biogeochemical model FESOM2.1–REcoM3 (Gürses et al., 2023). This open-source marine biogeochemistry model allows for regional grid refinement, which improves the spatial and temporal representation of ocean biogeochemical processes, such as the evolution of phytoplankton blooms. This provides the basis for future high-resolution and species-resolved PMOA modelling stud-

ies to improve the model representation and understanding of marine aerosols and their interactions with different cloud types.

In this work, the so-extended aerosol–climate model is thoroughly evaluated against observations worldwide, and the results are analysed globally in terms of temporal and spatial patterns. Through a component-specific description for ground-based observations, a comprehensive assessment of the total PMOA can be achieved.

The paper is organized as follows. Section 2 introduces the approach considered to compute the organic aerosol mass fraction and the concentration of the biomolecules in the ocean. Section 3 presents a description of the aerosol–climate model, the aerosol model setup, and experiments. Section 4 describes the observational data used for the evaluation. Sections 5 and 6 discuss the model results and the comparison with measurements focusing on marine biomolecules at the sea surface and the associated aerosol emissions and transport, respectively. Finally, Sect. 7 summarizes and draws the conclusions of this work.

## 2 Modelling marine organic aerosol emissions and marine biomolecules

This section outlines the method used to determine the organic aerosol mass fraction and quantify biomolecule concentrations in the ocean, which is used in the aerosol–climate model simulations to account for species-resolved PMOA. To represent the mass fraction in marine nascent aerosol, we base our calculations on OCEANFILMS (Organic Compounds from Ecosystems to Aerosols: Natural Films and Interfaces via Langmuir Molecular Surfactants; Burrows et al., 2014). For the present study, we included minor adaptations to the scheme. A detailed description of the assumptions made here together with the calculation of the marine biomolecule groups in the ocean is given in the following sections. Figure 1 shows a condensed illustration of the model components of this study for all compartments and encapsulates what is presented in Sects. 2–4. In addition, the computed and analysed parameters in the results sections are also included in Fig. 1.

### 2.1 PMOA emission parameterization

OCEANFILMS is a modelling framework that represents the sub-micron organic mass fraction in sea spray aerosol (air–sea interface compartment of Fig. 1). It is based on the Langmuir isotherm to represent the adsorption at bubble surfaces of the marine organic matter, which is apportioned into several classes. They include lipid-, polysaccharide-, protein-, humics-, and processed-like mixtures. The last two, humics- and processed-like mixtures, describe the recalcitrant DOC at the ocean surface, which is the DOC fraction that accumulates due to its resistance to rapid bacterial degradation

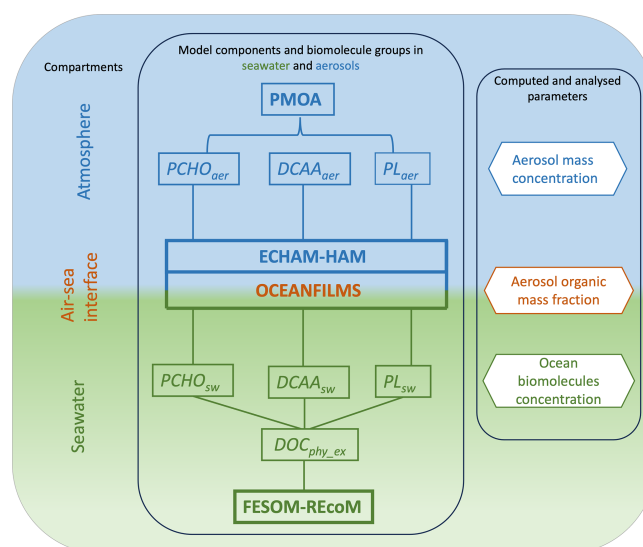


**Figure 1.** Schematic of the main modelling components considered in this study for simulating the biomolecules in seawater and their transfer to the atmosphere. Note that FESOM2.1–REcoM3 model data are used in offline mode and the modelled biomolecule groups serve as bottom boundary conditions of the integrated component OCEANFILMS + ECHAM6.3–HAM2.3. See Table 2 for the compound abbreviations.

(Hansell et al., 2012). These classes possess differing physicochemical characteristics: molar weight ( $MW_i$ ), surface area ( $A_i$ ), carbon concentration in seawater ( $C_i$ ), and Langmuir adsorption ( $\alpha_i$ ).  $C_i$  and  $\alpha_i$  regulate the bubble fractional surface coverage ( $\theta_i$ ). Note that  $i$  stands for the different classes. In combination with the bubble coating parameter ( $n = 2$ , equivalent coverage of the interior and exterior of the bubble), the mass on the bubble surfaces ( $M_i$ ) for each class can be computed as

$$M_i = n\theta_i \frac{MW_i}{A_i}. \quad (1)$$

Since PMOA and sea salt (SS) are emitted together, they make up the total mass of sea spray aerosol ( $M_{SSA}$ ). The organic mass fraction ( $OMF_i$ ) is then calculated based on the mass per bubble surface area of the individual macromolecule group ( $M_i$ ) and of sea salt ( $M_{SS}$ ):

$$M_{SSA} = M_i + M_{SS}, \quad (2)$$

$$OMF_i = \frac{M_i}{M_i + M_{SS}}, \quad (3)$$

where  $M_{SS}$  is assumed to be constant with a value of  $3.59 \times 10^{-3} \text{ g m}^{-2}$ .

The organic carbon aerosol enrichment is a result of the differing properties of the macromolecules in seawater that regulate their transfer to the atmosphere (Burrows et al., 2014). Despite lipids having the lowest concentration in the ocean, their surface affinity and competitive adsorption

favour their presence at the air–water interface (Frka et al., 2012) leading to higher aerosol enrichment compared to other macromolecules. Polysaccharide and protein surface affinity, on the other hand, is lower, limiting their transfer to the aerosols, with enrichment factors 2 orders of magnitude smaller than that for lipids (van Pinxteren et al., 2023). Lastly, humic- and processed-like mixtures have very low surface affinity, and, compared to the other classes, their contribution to the marine organic aerosol mass fraction may be negligible (Burrows et al., 2014). Hence, neglecting the recalcitrant portion of DOC will not impact the OMF estimations and is therefore not considered in this study.

In the current study we account for the presence of three main biomolecule groups that represent a portion of the lipid-, protein-, and polysaccharide-like classes. We focus on the contribution of extracellular DOC from phytoplankton, apportioning the organic matter into the most abundant biomolecule groups in seawater based on a closure approach that will be introduced in Sect. 2.3 (seawater compartment in Fig. 1). In this respect, our approach differs from Burrows et al. (2014), who considered the DOC primarily generated via cell lysis to compute the ocean concentration of the aforementioned groups. All parameters used for the computation of the main biomolecule groups in this work, however, are identical to those used in Burrows et al. (2014). They describe operational laboratory compounds selected to represent the ocean macromolecules and are shown in Table 1. These parameters could be refined in future studies to better characterize the biomolecule groups presented in this study.

In the following sections, we introduce the different components and considerations to compute each marine biomolecule group's ocean concentration. Firstly, we describe the ocean biogeochemistry model selected, which represents the DOC in the ocean. Later, we explain our closure approach to compute the marine organic groups based on the model tracers.

## 2.2 Marine biogeochemistry model

The upper-ocean biochemistry was simulated by the Regulated Ecosystem Model (REcoM3) coupled to the general circulation and sea ice Finite-Element/volume Sea ice–Ocean Model (FESOM2.1). FESOM2.1 is an unstructured-mesh ocean circulation model with high spatial resolution in dynamically active regions while including the remainder of the global ocean at a coarse resolution (Wang et al., 2014; Danilov et al., 2017; Koldunov et al., 2019). REcoM3 describes the ocean biogeochemistry in terms of the physical and biological carbon cycle with two phytoplankton and two zooplankton functional types, nutrients, dissolved as well as particulate organic matter, and detritus. The phytoplankton metabolic processes are regulated via non-linear limiter functions based on the variable, intracellular nitrogen-to-carbon ratio (N:C ratio) following Geider et al. (1998) and modified for REcoM3 in Schourup-Kristensen et al. (2014). These

functions regulate the nitrogen uptake and carbon exudation according to the N:C ratio (see Sect. A3.6 in Gürses et al., 2023, and Sect. A6.1 in Schourup-Kristensen et al., 2014).

Phytoplankton carbon is considered to partly exude organic carbon as dissolved carboxylic-acid-containing polysaccharides (PCHO) alongside other dissolved organic carbon molecules (Engel et al., 2020; Arnosti et al., 2021). PCHO and their aggregation product transparent exopolymer particles (TEPs) were included in REcoM version 1 by Schartau et al. (2007) and re-introduced for REcoM version 3 in the simulation used here, based on a mesocosm experiment by Engel et al. (2004), where the aggregation parameter choice itself is constrained by a mesocosm experiment of diatoms (Engel et al., 2002). A parameter optimization was successfully conducted by Schartau et al. (2007) and validated with a second mesocosm experiment of coccolithophores (Engel et al., 2004). Additionally, the parameter values fit with observational studies (Table 1 in Engel et al., 2004). This configuration is being assessed for the Arctic Ocean in a concurrent investigation. A detailed description and assessment of the REcoM version 3 performance on the global scale is available in Gürses et al. (2023).

The FESOM2.1–REcoM3 simulation was conducted for the period 1958–2019 on the so-called fARC mesh (<https://gitlab.awi.de/fesom/farc>, last access: 5 August 2024) with 4.5 km resolution in the Arctic Ocean, north of 60° N (Wekerle et al., 2017; Wang et al., 2018; Schourup-Kristensen et al., 2018). The global mesh resolution gradually decreases from the poles towards the Equator, the subtropical waters having the coarsest resolution of about 120 km (Schourup-Kristensen et al., 2018). Over the Equator and Southern Ocean, the resolution is relatively higher, between 30–40 km.

The simulation was forced with the atmospheric reanalysis data sets of JRA55-do v.1.4.0 (Tsujino et al., 2018) and initialized from temperature and salinity fields of the Polar Science Centre Hydrographic Climatology (Steele et al., 2001), as well as from initial fields of dissolved inorganic nitrogen and dissolved silicic acid concentration from the World Ocean Atlas climatology (Garcia et al., 2019a, b) and dissolved inorganic carbon as well as total alkalinity from the Global Ocean Data Analysis Project (GLODAP) version 2 (Lauvset et al., 2016). Monthly output was retrieved for the period of 1990–2019, the preceding years being considered as spin-up for the biological processes.

To obtain surface fields, we initially interpolated FESOM2.1–REcoM3 results from the original unstructured mesh to a regular grid of approximately 30 km (0.25°) horizontal resolution and calculated a volume-weighted mean for each grid cell over the upper 30 m of the water column. Finally, the biogeochemical model output and derived biomolecules in the ocean were interpolated to the ECHAM6.3–HAM2.3 grid and used as the bottom boundary condition of the aerosol model.

**Table 1.** Physicochemical parameters of the three ocean macromolecules considered in OCEANFILMS from Burrows et al. (2014).

Species	Molecular weight ( $MW_i$ in $\text{g mol}^{-1}$ )	Mass per area at surface saturation ( $\frac{MW_i}{A_i}$ in $\text{g m}^{-2}$ )	Langmuir adsorption parameter ( $\alpha_i$ in $\text{m}^3 \text{mol}^{-1}$ )
Polysaccharides	250 000	0.1375	90.58
Proteins	66 463	0.00219	25 175
Lipids	284	0.00259	15 205

**Table 2.** List of abbreviations of the most relevant aerosol and seawater compounds considered in the present study.

General terms	
PCHO	Dissolved carboxylic acid containing polysaccharides
DCAA	Dissolved combined amino acids
PL	Polar lipids
Seawater	
DOC	Dissolved organic carbon
DOC <sub>phy_ex</sub>	DOC fraction exuded by phytoplankton
PCHO <sub>sw</sub>	PCHO in seawater
DCAA <sub>sw</sub>	DCAA in seawater
PL <sub>sw</sub>	PL in seawater
DCCHO <sub>sw</sub>	Dissolved combined carbohydrates
PG <sub>sw</sub>	Dissolved phosphatidylglycerol
TEPs	Transparent exopolymer particles
Aerosols	
PMOA	Primary marine organic aerosol
OA	Organic aerosol
OC	Organic carbon
OM <sub>aer</sub>	Organic mass in aerosol
SSA	Sea spray aerosol
SS	Sea salt
PCHO <sub>aer</sub>	PCHO in aerosol particles
DCAA <sub>aer</sub>	DCAA in aerosol particles
PL <sub>aer</sub>	PL in aerosol particles
CCHO <sub>aer</sub>	Combined carbohydrates
CAA <sub>aer</sub>	Combined amino acids
PG <sub>aer</sub>	Phosphatidylglycerol

### 2.3 Organic biomolecules in seawater

The main sources of dissolved organic matter in seawater are phytoplankton exudates, carbon release via cell lysis, zooplankton grazing on phytoplankton, and zooplankton excretion (Carlson, 2002). Additionally, DOC also significantly forms from particulate organic carbon biological degradation (Repeta, 2015). From these sources, phytoplankton carbon exudation is considered a significant part of phytoplankton primary production (Myklestad, 2000). The most abundant components measured in extracellular carbon released by phytoplankton are carbohydrates (mono-, oligo-, and polysaccharides), proteinogenic compounds (amino acids, proteins, and peptides), lipids (fatty acids and polar lipids such as phosphoglycerides and glycosylglycerides), and to a

lesser degree organic acids (Lancelot, 1984; Yongmanitchai and Ward, 1993; Harwood and Guschina, 2009). Among these, polysaccharides, free and combined amino acids, and polar lipids represent the main biomolecule groups in the phytoplankton extracellular products (Parrish and Wangersky, 1987; Parrish et al., 1993, 1994; Obernosterer and Herndl, 1995; Engel et al., 2004; Arnosti et al., 2021).

These biomolecules can be measured both in seawater and in the aerosol phase (Kuznetsova et al., 2004; Zeppenfeld et al., 2020; Triesch et al., 2021b; van Pinxteren et al., 2023). In the present study we assume the aforementioned groups to be characterized by the biomolecules that form the majority of the phytoplankton extracellular carbon: dissolved carboxylic acid containing polysaccharides (PCHO<sub>sw</sub>), dissolved combined amino acids (DCAA<sub>sw</sub>), and phospholipids

and glycolipids as polar lipids ( $PL_{sw}$ ) in seawater. The DOC fraction exuded by phytoplankton ( $DOC_{phy\_ex}$ ) is resolved in the FESOM2.1-REcoM3 model (Gürses et al., 2023), and we use it to derive the biomolecule groups. Based on these premises, we compute the ocean surface concentration of the biomolecules by apportioning the  $DOC_{phy\_ex}$  into the contribution from each group:

$$DOC_{phy\_ex} = C_{PCHO_{sw}} + C_{PL_{sw}} + C_{DCAA_{sw}} + Res. \quad (4)$$

$C_{PCHO_{sw}}$ ,  $C_{PL_{sw}}$ , and  $C_{DCAA_{sw}}$  refer to the surface ocean concentration of each group (seawater compartment in Fig. 1), while  $Res$  is the residual that will be attributed to compounds not included in the three main classes, with contributions ranging between 9% and 38% of  $DOC_{phy\_ex}$  (Hellebust, 1965; Al-Hasan and Coughlan, 1976).

In the FESOM2.1-REcoM3 model, the DOC phytoplankton excretion rate ( $DOC_{phy\_ex\_rate}$ ) describes the phytoplankton release per unit of time and is considered a source term in the semi-labile DOC (see Eqs. A42 and A55 in Gürses et al., 2023):

$$DOC_{phy\_ex\_rate} = (\epsilon_{phy}^C f_{lim,phy} PhyC_{phy} + \epsilon_{dia}^C f_{lim,dia} PhyC_{dia}). \quad (5)$$

PhyC refers to the phytoplankton carbon concentration, and the sub-indices “phy” and “dia” refer to small and diatom phytoplankton groups, respectively.  $\epsilon$  is the excretion constant of organic carbon ( $d^{-1}$ ), and  $f$  is a limiter function that downregulates the phytoplankton excretion when the nitrogen quota ( $qN : C$ ) becomes too high.

To represent acidic dissolved polysaccharides in seawater ( $PCHO_{sw}$ ) and TEPs, which are gel-like particles formed from  $PCHO_{sw}$ , Schartau et al. (2007) developed a formulation based on the extracellular production of organic carbon from phytoplankton and aggregation processes (see previous section). Simulated  $PCHO_{sw}$  accounts for approximately 63% of exuded organic carbon by small phytoplankton and diatoms, representing the majority of the modelled DOC. According to laboratory studies, dissolved polysaccharides account for the highest fraction of exuded carbon by phytoplankton, and their contribution to the exuded carbon ranges from 47% to 90% (Mykkestad, 1995; Biersmith and Benner, 1998; Hama and Yanagi, 2001). It is therefore assumed that

$$C_{PCHO_{sw}} = PCHO_{sw} \Big|_{FESOM-REcoM}. \quad (6)$$

Overall, lipid material in phytoplankton-exuded DOC ranges from 2.8% to 10.3% (Hellebust, 1965; Billmire and Aaronson, 1976). Considering that on average  $\delta = 5\%$  of the  $DOC_{phy\_ex\_rate}$  will be attributed to the extracellular  $PL_{sw}$  production rate ( $S_{PL_{sw}}$ ), the ocean surface concentration can be approximated as  $S_{PL_{sw}}$  multiplied by the lifetime ( $\tau$ ) of lipids in seawater after release:

$$C_{PL_{sw}} = \tau S_{PL_{sw}}, \quad (7)$$

with

$$S_{PL_{sw}} = \delta DOC_{phy\_ex\_rate}. \quad (8)$$

Lipids are short-lived compounds, whose turnover time is just a few days (Hopkinson et al., 2002; Karl and Björkman, 2015). Sensitivity studies, performed with typical turnover times of  $PL_{sw}$  between 4 and 10 d (Karl and Björkman, 2015), led to the best agreement with observation for turnover rates of 8 d.

$C_{DCAA_{sw}}$ , on the other hand, was determined differently. Based on various concentration values measured in ambient seawater from different sites (see also the measurement description below), we calculated the ratio of observed dissolved combined carbohydrates ( $DCCHO_{sw}$ ) and  $DCAA_{sw}$  (from 31 seawater samples). A median value of  $ratio = 0.3 \pm 0.08$  was obtained and is used here to compute  $DCAA_{sw}$  in the ocean based on  $PCHO_{sw}$  modelled concentration. Nevertheless, employing this method results in the estimated  $DCAA_{sw}$  encompassing both extracellular and intracellular carbon derived from phytoplankton. Consequently, the modelled concentrations reflect the aggregate of these two  $DCAA_{sw}$  formation mechanisms, as it is not feasible to differentiate the relative contribution of extracellular carbon released by phytoplankton based on observational data. Hence, in our approach,  $DCAA_{sw}$  will be the sole group for which the sources may include contributions beyond extracellular release by phytoplankton ( $C'_{DCAA_{sw}}$ ).

$$C'_{DCAA_{sw}} = ratio \cdot C_{PCHO_{sw}} \quad (9)$$

Considering that carbohydrates constitute a significant portion of semi-labile DOC, with turnover times ranging from months to years, the computed  $DCAA_{sw}$  will also contribute to this fraction. Therefore, the labile or refractory component of  $DCAA_{sw}$  is not included in the current study.

Values found in the literature indicate that extracellular amino acids represent 1.5% to 7% of exuded DOC (Mykkestad et al., 1972; Mague et al., 1980; Granum et al., 2002). Presuming that extracellular  $DCAA_{sw}$  represents nearly 5%, together with  $PCHO_{sw}$  and  $PL_{sw}$ , the biomolecules constitute approximately 73% of exuded organic carbon by phytoplankton groups in FESOM2.1-REcoM3, where dissolved acidic polysaccharides account for the highest fraction. The residual 27% may include other lipid-, polysaccharide-, and protein-like compounds, as well as organic acids or other unknown components.

## 2.4 Approximations of phytoplankton extracellular carbon release

The abundance of the biomolecule exuded by phytoplankton exhibits a significant temporal and spatial variability, primarily influenced by phytoplankton growth phase and nutrient availability (Mykkestad, 2000). Other studies have demonstrated that the carbon exudation also differs among species

(Hellebust, 1965; Wolter, 1982; Wetz and Wheeler, 2007). Furthermore, intense light conditions induce abrupt modifications in the extracellular release, with the proportion of carbon incorporated into cells remaining approximately constant in comparison to that exuded by phytoplankton, as documented by Mague et al. (1980).

During phytoplankton growth, extracellular carbon release is influenced by nutrient conditions. The exudation tends to be slightly higher for the rapidly growing than for the stationary phase (Mykkestad et al., 1989). The exuded products differ for every case and phytoplankton species. For instance, higher levels of extracellular polysaccharides and free amino acid release were observed during phosphorus-limited conditions compared to balanced nutrient conditions (Obnersterer and Herndl, 1995). In contrast, whereas proteinogenic compounds and free amino acids decrease under nitrogen depletion (Granum et al., 2002), extracellular polysaccharides are significantly favoured (Mykkestad, 1995).

Biogeochemical models often parameterize the phytoplankton carbon exudation by setting a constant phytoplankton biomass loss per day (Thornton, 2014). This fraction is set to 10 % for both phytoplankton groups in FESOM2.1–REcoM3 (Gürses et al., 2023). Moreover, the exuded carbon is regulated by a limiting factor as a measure of nutrient availability, which depends entirely on the carbon and nitrogen quota, and, lastly, it is independent of light conditions (see Eq. 5).

Furthermore, since simplifications are required for the global biogeochemistry model, diatoms and small phytoplankton do not distinguish the species within those groups. Therefore, the distinct characteristics of each phytoplankton culture, which exhibits an unequal distribution in seawater and extracellular carbon release levels (Granum et al., 2002), cannot be captured. Therefore, the values utilized in the present study to estimate the contribution of each biomolecule to the extracellular DOC released by phytoplankton in the ocean were either averaged across multiple laboratory studies or approximated, thus limiting them to known measured quantities in the literature (Hellebust, 1965; Billmire and Aaronson, 1976; Mague et al., 1980; Mykkestad, 1995; Biersmith and Benner, 1998; Hama and Yanagi, 2001; Granum et al., 2002).

### 3 Global aerosol–climate simulations

#### 3.1 The ECHAM6.3–HAM2.3 model

Aerosol–climate models represent aerosol emission, transport, wet and dry deposition, and direct and indirect radiative effects in the earth system. In this study, we used the model ECHAM6.3–HAM2.3 (Tegen et al., 2019), which combines the atmospheric general circulation model ECHAM6.3 (Stevens et al., 2013) with a spectral transform dynamical

core (Lin and Rood, 1996) and the Hamburg Aerosol Module (HAM2.3) (Stier et al., 2005).

The aerosol microphysics module, HAM, is based on the M7 aerosol model (Vignati et al., 2004; Stier et al., 2005). The aerosol species considered in the model are sulfate ( $\text{SO}_4$ ), organic carbon (OC), black carbon (BC), mineral dust (DU), and sea salt (SS). For OC, BC, and  $\text{SO}_4$ , emissions are initially prescribed from anthropogenic sources and biomass burning emission inventories and from volcanic eruptions. Wind-driven DU and SS emission fluxes from desert and the ocean, respectively, are calculated online in the model. Additionally, dimethyl sulfide (DMS) is emitted from the marine biosphere.

Aerosol species are divided into two groups of soluble and insoluble aerosol particles for a total of seven log-normal classes according to a predefined four-group aerosol size spectrum (Table 3). The aerosol mass and number concentration is predicted for each mode. The log-normal distribution depends on the aerosol number, median radius, and standard deviation. Modes exist as soluble or insoluble. All species in a soluble mode are considered to be internally mixed, meaning that every particle is actually a mixture of all the species within the mode.

The PMOA compounds are treated as separate tracers and included in the model as three new individual species (atmosphere compartment in Fig. 1) to the soluble accumulation and coarse modes (see Table 3). These organic groups do not contribute to but share the microphysical and optical particle properties of the OC tracer. Since the model does not represent sea spray emission for the Aiken mode, PMOA is initially emitted solely into the accumulation mode. Then, the particles grow by coagulation or condensation, increasing the mean geometric radii and eventually transitioning to a larger mode.

HAM includes aerosol transformation processes such as the nucleation of sulfuric acid and water droplets, coagulation and condensation of sulfuric acid, and water uptake. In addition, deposition, aerosol interactions with clouds, and radiation are also accounted for. The updated version of HAM2.3 encompasses several improvements to the aerosol processes and emission (Tegen et al., 2019) as well as to aerosol–cloud interactions (Lohmann and Neubauer, 2018).

The two-moment cloud microphysics scheme in ECHAM6.3–HAM2.3 follows Lohmann et al. (2007) and Lohmann and Hoose (2009). It allows for in-cloud and below-cloud scavenging aerosol processes for liquid, ice, and mixed-phase clouds. The cloud droplet activation is based on the Köhler theory by Abdul-Razzak and Ghan (2000). ECHAM6.3 has implemented a rapid radiative transfer model (PSrad/RRTMG) to represent the radiative interaction with aerosols and clouds (Pincus and Stevens, 2013).

**Table 3.** Aerosol modes and compounds in HAM.  $r$  denotes the radius of the respective particle size range and  $\sigma$  the standard deviation.

Size mode/size range ( $\mu\text{m}$ )	Soluble/internally mixed	Insoluble/externally mixed
Nucleation <sup>a</sup> ( $r \leq 0.005$ )	SO <sub>4</sub>	
Aitken <sup>a</sup> ( $0.005 < r \leq 0.05$ )	SO <sub>4</sub> , OC, BC	OC, BC
Accumulation <sup>a</sup> ( $0.05 < r \leq 0.5$ )	SO <sub>4</sub> , OC, BC, DU, SS, PCHO <sub>aer</sub> , DCAA <sub>aer</sub> , PL <sub>aer</sub>	DU
Coarse <sup>b</sup> ( $r > 0.5$ )	SO <sub>4</sub> , OC, BC, DU, SS, PCHO <sub>aer</sub> , DCAA <sub>aer</sub> , PL <sub>aer</sub>	DU

<sup>a</sup>  $\sigma = 1.59$ . <sup>b</sup>  $\sigma = 2.0$ .

### 3.2 Emissions of sea spray aerosol

Marine aerosols emission flux is calculated based on Eq. (2), where PMOA and SS make the total sea spray mass. Thus, the emitted PMOA mass flux of each biomolecule group ( $i$ ) can be computed as

$$\text{PMOA}_{\text{mass flux}}(i) = \frac{\text{SS}_{\text{mass flux}} \cdot \text{OMF}_i}{1 - \text{OMF}_i}, \quad (10)$$

where OMF refers to the organic mass fraction parameterized based on OCEANFILMS (Burrows et al., 2014), as previously described.  $\text{SS}_{\text{mass flux}}$  is the mass flux of sea salt emitted in ECHAM6.3–HAM2.3. The model includes a range of widely used sea salt emission schemes, including, among others, Guelle et al. (2001), Gong (2003), and Long et al. (2011). The default configuration is considered for the current study and follows Long et al. (2011) with sea surface temperature correction according to Sofiev et al. (2011). This combination showed the best agreement with observed surface sea salt aerosol concentration and particle size distribution across multiple marine sites in the model evaluation study by Tegen et al. (2019).

Following Burrows et al. (2022), we assume that PMOA is internally mixed and the number and fluxes added onto sea salt. The authors performed sensitivity studies with various combinations of the mixing state of PMOA with sea salt in the Energy Exascale Earth System Model (E3SM). Their findings indicate that the chosen configuration provided a better seasonal representation of organic mass and aerosol concentration compared to observations.

### 3.3 Experimental setup

The aerosol–climate model simulations are performed at T63 (approx.  $1.875^\circ \times 1.875^\circ$ ) horizontal resolution with a total of 47 vertical levels, which resolves the atmosphere from the surface up to 0.01 hPa. The model is run in nudged mode with the re-analysis data from the European Centre for Medium-Range Weather Forecasts (ECMWF) known as ERA-Interim.

Sea ice concentration (SIC, as the percentage of area covered by ice) and sea surface temperature (SST) monthly mean values from the Atmospheric Model Intercomparison Project (AMIP) (Taylor et al., 2000) are used as boundary conditions for the model experiments. The simulations cover a period of 10 years (2009–2019) in which aerosol measurements were available. A spin-up time of 4 months and an output frequency of 12 h were considered.

Two experiments, without and with simulated PMOA as a tracer in the model, were performed, hereafter referred to as SPMOAoff and SPMOAon, respectively. The SPMOAoff simulation only accounts for the fraction of sea salt in sea spray aerosol, whereas the SPMOAon utilizes the biomolecule ocean surface concentration as bottom boundary conditions to compute the marine organic aerosol fraction in addition to the sea salt. For consistency with the biogeochemistry-model-predicted sea ice, an adjustment of SIC and SST within the sea salt emission scheme is considered, intending to avoid ambiguities. To ensure comparability with previously published results of the aerosol–climate model (Tegen et al., 2019) and avoid re-tuning, the AMIP data are retained for the simulations. A mask is applied to determine when FESOM2.1–REcoM3 model SIC and SST values replace or modify AMIP data. Whenever ice-free ( $\text{SIC} < 10\%$ ) conditions for the marine biogeochemistry model are satisfied, the AMIP SIC values are updated during runtime to 0% and SST is replaced by that from FESOM2.1–REcoM3. Note that the mask only applies when the sea salt emission scheme is called, thus not affecting the rest of the globe.

## 4 Observations for model evaluation

In this section, we will discuss the measurement data selected for the model evaluation. We present the seawater sample data of measured marine compounds that are being compared with the concentration of marine biomolecules in the

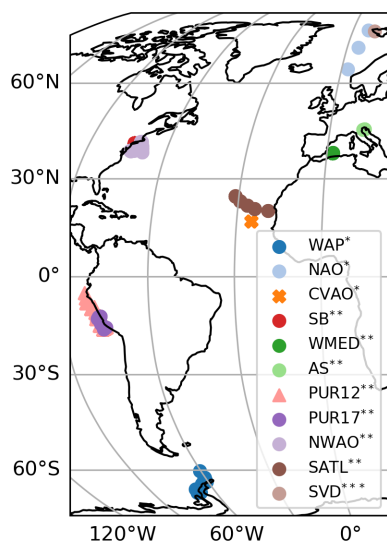


**Figure 2.** Station locations for seawater samples and marine aerosol measurements. The circles, triangles, and cross markers indicate the stations for which one, two, and three compounds were measured, respectively. The asterisks indicate the type of data available at each location: \* – seawater and aerosol; \*\* – only seawater; \*\*\* – only aerosol. See Table 4 for the location abbreviations. The most relevant information regarding the data can be found in Table 5.

ocean. Likewise, we validate the offline-computed organic mass fraction and simulated aerosol concentration of each group with analogous compounds from observations. This species-wise evaluation will assess how well the models can represent the different biomolecules in seawater and the atmosphere. Nonetheless, the data are primarily accessible for specific locations and do not provide an overview of marine organics' abundance in remote oceanic areas. Thus, as the final dataset for model evaluation, in situ airborne organic aerosol concentration measurements with extensive coverage of most oceanic regions are used to provide a more thorough evaluation of PMOA.

#### 4.1 Seawater samples and in situ ground-based measurements

Modelled estimates of ocean surface concentration of biomolecule and aerosol OMF and concentration (Fig. 1) are compared to bulk seawater samples and aerosol observations from various stations worldwide (Fig. 2). Table 5 summarizes the most relevant information of these marine and aerosol measurements. The comprehensive collection of observational data in this study was compiled considering similar sampling techniques and laboratory instruments to detect and measure the concentration of the organic compounds. Details on the compounds selected for the model evaluation are introduced in this section. Additionally, a brief description of the interpolation of model results for the comparison is presented.

Seawater samples were collected between 10 cm and 3.5 m depth, often with a plastic or glass bottle to collect the water at a specific depth. For simplicity, only measurements from the open ocean without sea ice were included. Whereas the model mostly represents the biomolecule production from phytoplankton, the in situ measurements do not allow us to trace back the production mechanism of these groups. Hence, modelled quantities may represent a portion of the measured biomolecules. Although the measurements are not strictly comparable to the model results, they are good indicators to validate the modelled quantities.

We therefore selected analogous components for the model evaluation. Seawater measurements of dissolved combined carbohydrates ( $DCCCHO_{sw}$ ), dissolved combined amino acids ( $DCAA_{sw}$ ), and dissolved phosphatidylglycerol ( $PG_{sw}$ ) were chosen for comparison with modelled  $PCHO_{sw}$ ,  $DCAA_{sw}$ , and  $PL_{sw}$ , respectively.  $DCAA_{sw}$  is considered to be approximately equal to the measured hydrolysable dissolved combined amino acids (DHAA). On the other hand, the selection of  $PG_{sw}$  was based on the fact that phytoplankton extracellular lipids are essentially formed by phosphoglycerides and glycosylglycerides (Yongmanitchai and Ward, 1993; Guschina and Harwood, 2009). Moreover, the presence of this compound in seawater is often correlated to phytoplankton (Triesch et al., 2021b).

Additionally, aerosol data were carefully cleaned, including only those for which a correlation with marine biological activity has been reported. Aerosol samples were collected in filters exposed at heights between 4 and 50 m a.m.s.l. For the aerosols, we selected the same tracers that are linked to the marine amounts. Observations of combined carbohydrates ( $CCHO_{aer}$ ), amino acids ( $CAA_{aer}$ ), and  $PG_{aer}$  are available for comparison to the simulated aerosol concentration and organic fraction of  $PCHO_{aer}$ ,  $DCAA_{aer}$ , and  $PL_{aer}$ , respectively (Table 5).

OMF for each group is available from OCEANFILMS. On the other hand, for the measurements, we derived OMF based on the observed marine aerosols and sea salt mass, which was estimated as a constant rate ( $1/0.3061$ ) of sodium ( $Na^+$ ) concentration (Seinfeld and Pandis, 2006). Lastly,  $OM_{aer}$  is derived from the measured OC, considering a ratio of  $OM : OC = 2$  of remote region aerosols following Turpin and Lim (2001). Nonetheless, this ratio may vary as aerosol particles age in the atmosphere and depending on the content of water-soluble organic material (Sciare et al., 2005; Facchini et al., 2008).

For the model evaluation, simulated results are interpolated to the observation sites using a cubic-triangular-based interpolator, a suitable method to detect and account for gradients in the data. Note that we use monthly ocean values, which do not capture the spatial and temporal variability in marine biogeochemistry within a month (e.g. CVAO seawater samples in Triesch et al., 2021b). This can affect cases where the quantity of samples is limited and restricted to a single location, such as CVAO, where the interpolated

ocean concentrations remain nearly identical. Nevertheless, a comprehensive examination of the daily modelled  $\text{PCHO}_{\text{sw}}$  against observations (not shown) for the summer of 2017 revealed an overall lower agreement with water samples than when utilizing monthly mean values.

For the aerosol comparison, we interpolated the near-surface model vertical level aerosol concentration to the coordinates of the stations. Most stations are land-based, except for NAO and WAP, in which aerosols were sampled on board of a ship. For these cases, we interpolated the simulated values for the ship trajectories and averaged over a starting and ending point in accordance with observations. For Svalbard, filters were exposed for at least 6 d. Hence, interpolated model values were averaged over these period for the comparison with observations.

## 4.2 Aircraft observations of organic aerosols

To provide an overview of the model's capability to represent PMOA in remote oceanic regions where ground-based measurements are not available, we compare the simulated PMOA concentrations with aircraft observations over the ocean regions that are least affected by organic carbon from non-marine sources. Mass concentrations of organic aerosols (OAs) from the Atmospheric Tomography (ATom, <https://espoarchive.nasa.gov/archive/browse/atom>, last access: 1 August 2024) campaigns of the US National Aeronautics and Space Administration (NASA) are used for the comparison to the aerosol model results. Information regarding the different instruments on board the aircraft, measuring aerosol quantities, can be found at the official website. The aircraft flew mostly over open-ocean areas and within the Arctic region. The data are available at a temporal resolution of approximately 15 min.

Some studies analysing ATom data indicate that PMOA could significantly contribute in remote oceanic regions to the OA (Pai et al., 2020). Following Pai et al. (2020), we selected the near-surface levels from ATom data (heights under 1 km) limiting the comparison to the marine boundary layer, in which marine local sources should predominate. In an attempt to exclude organic aerosol from anthropogenic and biomass burning sources that mostly influence the Northern Hemisphere, we imposed a threshold to OA values and excluded those over  $0.2 \mu\text{g m}^{-3}$  (measured at standard temperature and pressure conditions: 273 K, 1 atm) as in the regime's classification by Pai et al. (2020). Figure 3a shows the data grouped by months after applying the aforementioned conditions. Any data collected inland, where primary marine aerosols have no impact, were excluded, reducing the dataset to the open-ocean or near-coastal regions. The majority of the data was measured in October 2017, followed by February of the same year and May 2018 (with a sample size of 64, 40, and 30 observations, respectively). The remaining cases comprise fewer than 12 observations. Since some of the flight

trajectories overlap, the Fig. 3a does not visually represent the actual number of samples for some cases.

To distinguish pristine regions that are most likely dominated by PMOA from those that are more anthropogenically influenced or more polluted, we only selected the flight legs for the model evaluation as shown in Fig. 3b. Northern Hemisphere aerosols, which are predominantly dominated by anthropogenic sources, biomass burning, and natural fires and would therefore mask the weaker signal of the PMOA, are thus excluded from the comparison (light gray locations in Fig. 3b).

For the evaluation of model results, the hybrid model vertical levels were transformed into pressure levels and linearly interpolated to the flight horizontal coordinates and altitude where the aerosols were sampled. Since the model output is only 12-hourly, we spatially interpolated the flight points, which laid within this 12 h range. This means that all flight coordinates between 00:00 (12:00) UTC and 12:00 UTC (00:00 UTC of next day) of a certain day are interpolated to the model output corresponding to the same day at 12:00 UTC (00:00 UTC of next day). Then, we derived daily averages of observational and modelled values and calculated the correlation coefficient and model bias for the whole dataset, accordingly. Additionally, model results were converted to standard conditions of temperature and pressure to meet the conditions, at which the ATom aircraft samples were measured.

## 5 Results and discussion

### 5.1 Geographical distribution of modelled biomolecules

Based on the FESOM2.1–REcoM3 model data and the calculations in Sect. 2.3, the three key marine biomolecules at the sea surface have an average spatial distribution as shown in Fig. 4a–c. In addition, Fig. 4d–f present the aerosol organic mass fraction (OMF) calculated with the OCEANFILMS scheme as considered in this study in an offline mode with the simulated ocean surface concentration as input data.

#### 5.1.1 Sea surface concentration of biomolecules

The global distribution of marine biomolecules exhibits distinct patterns for the semi-labile groups  $\text{PCHO}_{\text{sw}}$  and  $\text{DCAA}_{\text{sw}}$ , in contrast to the labile  $\text{PL}_{\text{sw}}$  group, due to their resistance to rapid microbial utilization.  $\text{PCHO}_{\text{sw}}$ , as the main extracellular product of phytoplankton, has a maximum concentration of up to  $8.4 \text{ mmol C m}^{-3}$ .  $\text{DCAA}_{\text{sw}}$  and  $\text{PL}_{\text{sw}}$  have values as high as 2.5 and  $1.28 \text{ mmol C m}^{-3}$ , respectively (see Fig. 4a, b).

$\text{PCHO}_{\text{sw}}$  and  $\text{DCAA}_{\text{sw}}$  show persistently high concentrations over tropical waters (Fig. 4a, b). This is linked to the strong stratification that prevents deep vertical mixing and remineralization. In addition, we also associate these

**Table 4.** List of abbreviations and coordinates of the locations of the measurement campaigns and observational stations used for the model evaluation.

Abbreviation	Meaning	Coordinates
WAP	Western Antarctic Peninsula	64–68° S, 60–69° W
NAO	North Atlantic Ocean	64–79° N, 2–8° E
CVAO	Cape Verde Atmospheric Observatory	16.9° N, 24.9° W
SB	Stony Brook Harbor	40.9° N, 73.2° W
WMED	Western Mediterranean	37.7–37.8° N, 1.9–2.2° E
AS	Adriatic Sea	44.9–45.1° N, 12.8–13.3° E
PUR12	Peruvian Upwelling Region 2012 campaign	5–16° S, 75–82° W
PUR17	Peruvian Upwelling Region 2017 campaign	12–75° S, 78–69° W
NWAO	Northwestern Atlantic Ocean	38–41° N, 69–73° W
SATL	Subtropical Atlantic	20–25° N, 19–31° W
SVD	Svalbard	78.9° N, 11.9° E

**Table 5.** Bulk water samples and aerosol measurements selected for the comparison with modelled biomolecule and aerosol tracers. Sea-water sampling techniques employed during each campaign of each molecule group are the same. The measurement techniques are high-performance anion exchange chromatography coupled with pulsed amperometric detection (HPAEC-PAD) for quantifying DCCHO<sub>sw</sub>, high-performance liquid chromatography (HPLC) for DCAA<sub>sw</sub>, and thin-layer chromatography with the flame ionization detection (TLC/FID) for PG<sub>sw</sub>. See Tables 2 and 4 for the compound and location abbreviations, respectively. References abbreviations: EG16 – Engel and Galgani (2016); vP23 – van Pinxteren et al. (2023); Z23 – Zeppenfeld et al. (2023); Z21 – Zeppenfeld et al. (2021); ME21 – Maßmig and Engel (2021); K02 – Kuznetsova and Lee (2002); K04 – Kuznetsova et al. (2004); R08 – Reinthaler et al. (2008); F19 – Feltracco et al. (2019); T21a – Triesch et al. (2021a); T21b – Triesch et al. (2021b); F11 – Frka et al. (2011). NA represents not available.

Compounds (seawater/aerosol)	Water samples/aerosol availability	Location	Depth (m)/height (m a.m.s.l.)	No. of observations	Date	References
DCCHO <sub>sw</sub> /CCHO <sub>aer</sub>	avail./NA	PUR12	0.2/–	39/–	Dec 2012	EG16
	avail./NA	PUR17	1–3.5/–	13/–	Apr, Jun 2017	ME21
	avail./avail.	CVAO	1/30	3/7	Sep, Oct 2017	vP23
	avail./avail.	NAO	1/25	3/3	May 2017	Z23
	avail./avail.	WAP	0.25/4, 18	18/16	Jan–Mar 2019	Z21
DCAA <sub>sw</sub> /CAA <sub>aer</sub>	avail./NA	SB	0.1/–	41/–	Feb–Sep 1999; Feb–Sep 2000	K02
	avail./NA	NWAO	0.15/–	22/–	Jun 2001	K04
	avail./NA	SATL	0.3/–	17/–	Sep, Oct 2004	R08
	avail./NA	WMED	0.3/–	5/–	Sep, Oct 2003	R08
	avail./NA	PUR12	0.2/–	31/–	Dec 2012	EG16
	NA/avail.	SVD	–/50	–/5	Apr–Jun 2015	F19
	avail./avail.	CVAO	–/30	–/7	Sep, Oct 2017	T21a
PG <sub>sw</sub> /PG <sub>aer</sub>	avail./avail.	CVAO	1/30	16/5	Sep, Oct 2017	T21b
	avail./NA	AS	0.5/–	6/–	Apr, Jun, Aug 2008	F11

patterns with the carbon-overflow hypothesis (Engel et al., 2004, 2020), in which the carbon exudation increases under nutrient-limiting conditions. In FESOM2.1–REcoM3, nitrogen is indeed the most limiting factor of small phytoplankton in the vast areas of tropical and subtropical waters (Schourup-Kristensen et al., 2014; Gürses et al., 2023). For polar regions, on the other hand, the model results have the lowest values during polar night. In the bloom period during northern hemispheric spring, the PCHO<sub>sw</sub> and DCAA<sub>sw</sub> concentrations in the Arctic rise to values slightly higher than 8 and 2.5 mmol C m<sup>−3</sup>, respectively (see Fig. B1d–e). For the Southern Ocean, however, the maximum tends to be lower, at 5.3 mmol C m<sup>−3</sup> for PCHO<sub>sw</sub> and 1.6 mmol C m<sup>−3</sup>

for DCAA<sub>sw</sub> (see Fig. B1a, b). The distinction can be attributed, among other factors, to the presence of significant river mouths in the Arctic, which serve as a significant source of nutrients for the polar waters that are not present in the Southern Ocean.

The greatest contributions of PL<sub>sw</sub> (Fig. 4c) are found in the equatorial upwelling region and polar waters (see Fig. B1). Lower values predominate in the subtropical gyres where carbon exudation is solely dominated by the small phytoplankton group. In contrast to the other biomolecules, the values are lowest in the tropics, while higher contributions are found in the Arctic and Antarctic waters during the bloom period (Fig. B1c, j). Lastly, the low quantities simu-

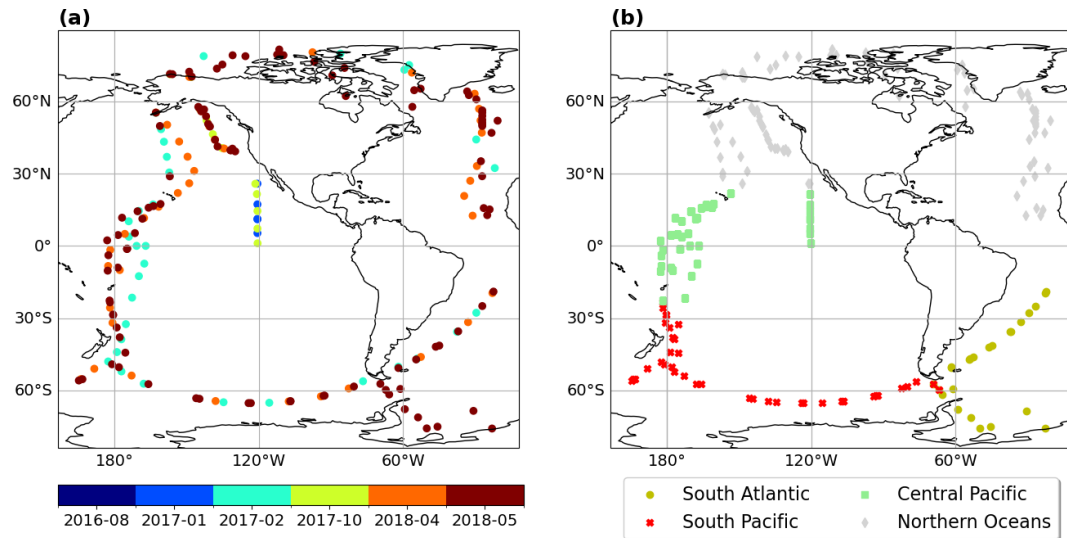


**Figure 3.** (a) Airborne organic aerosol particles grouped by days for diameters smaller than  $1\ \mu\text{m}$ , altitudes below  $1\ \text{km}$ , and concentrations smaller than  $0.2\ \mu\text{g s}^{-3}$ . (b) Colour-coded regions selected for the model evaluation. The northern ocean region potentially most influenced by long-range-transported aerosols is represented here for reference (in light grey) but excluded from the model evaluation analysis.

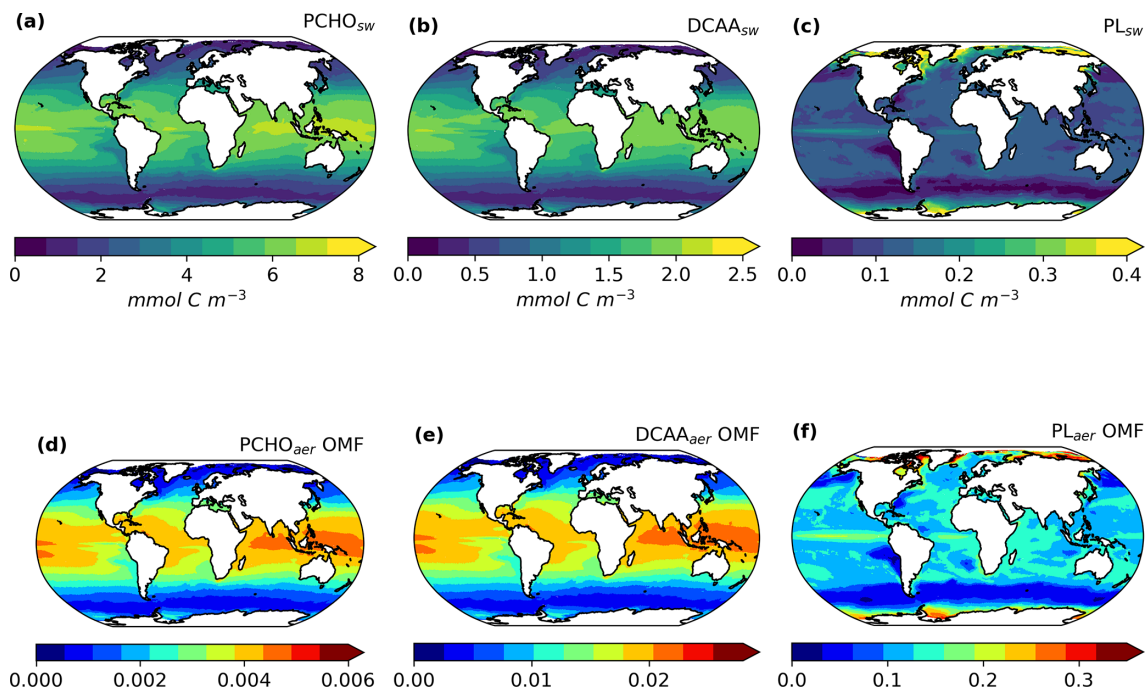


**Figure 4.** Maps of global-averaged (a–c) ocean carbon concentration of  $\text{PCHO}_{\text{sw}}$ ,  $\text{DCAA}_{\text{sw}}$ , and  $\text{PL}_{\text{sw}}$  and (d–f) offline-computed OMF of  $\text{PCHO}_{\text{aer}}$ ,  $\text{DCAA}_{\text{aer}}$ , and  $\text{PL}_{\text{aer}}$  as a multiannual mean for the period 1990–2019 for sea-ice-free conditions ( $\text{SIC} < 10\%$ ).

lated in the subtropical Pacific off the west coast of South America are common for all biomolecules. For this area, the dissolved inorganic nitrogen in the FESOM2.1–REcoM3 model has been excessively high compared to observations (Gürses et al., 2023). Additionally, the high nitrogen concentration also observed in the Southern Ocean could explain the low phytoplankton carbon exudation in this region. For this

case, the intracellular nitrogen quota of small phytoplankton is high. As a consequence, the limiting function in Eq. (5) downregulates the carbon excretion. Therefore, the modelled carbon phytoplankton exudation is minimal given the elevated availability of nitrogen in these areas.

In addition to the spatial patterns, the seasonality of biomolecules in the ocean was also analysed by region (Ta-

ble 6). All quantities are highest during hemispheric summer for the poles and subtropics (Fig. B1). For June–July–August, the total concentration of all biomolecules is on average  $3.72 \pm 1.74$  and  $0.55 \pm 0.23$   $\text{mmol C m}^{-3}$  for the Arctic and Southern Ocean, respectively. During December–January–February the concentration increases in the southern region ( $4.61 \pm 2.7$   $\text{mmol C m}^{-3}$ ) and declines in the Arctic seas ( $0.68 \pm 0.29$   $\text{mmol C m}^{-3}$ ). Whereas the concentrations of  $\text{PCHO}_{\text{sw}}$  and  $\text{DCAA}_{\text{sw}}$  drop by about 80 % during the polar night,  $\text{PL}_{\text{sw}}$  falls to almost zero (Table 6). The amplitude between seasons is nearly twice smaller for the subtropics compared to the poles. Nevertheless, total quantities are larger for subtropical waters with values of  $5.48 \pm 1.81$   $\text{mmol C m}^{-3}$  ( $3.75 \pm 2.02$   $\text{mmol C m}^{-3}$ ) and  $5.07 \pm 1.73$   $\text{mmol C m}^{-3}$  ( $2.9 \pm 1.9$   $\text{mmol C m}^{-3}$ ) during summer (winter) for the northern and southern high latitudes, respectively. In contrast, seasonal patterns diminish towards the Equator ( $7.9$   $\text{mmol C m}^{-3}$ ), where they are absent due to the intense solar radiation being a limiting factor rather than nutrient depletion (Fig. B1). To our knowledge, there have been scarcely any studies on the surface concentration of marine organic compounds relevant for aerosols and none on the modelling of the carbon groups presented here. Two examples that closely resemble this work are the studies conducted by Ogunro et al. (2015) and Burrows et al. (2014). Among other groups and bio-indicators of ocean marine biological activity, Ogunro et al. (2015) presented the abundance of polysaccharide-, protein-, and lipid-like mixtures. Burrows et al. (2014) based their OCEANFILMS calculations on the macromolecule quantities, similarly derived from the same biogeochemistry model as in Ogunro et al. (2015). These two research studies assumed that the primary source of total DOC was cell lysis, and based on this assumption, they calculated the concentration of the macromolecular groups at the sea surface. Their computed quantities encompass a broader group than those examined in our study. Polysaccharides were assumed to be equal to the semilabile dissolved organic carbon pool from a biogeochemical model (Ogunro et al., 2015; Burrows et al., 2014), which is equivalent to the  $\text{DOC}_{\text{phy-ex}}$  from FESOM2.1–REcoM3 in our study. With this assumption, other potential sources of polysaccharides are included, leading to higher values than in this work (up to 10-fold) and slightly different geographical distribution. Nonetheless, similar to our results, the abundance of proteins and polysaccharides is more pronounced in lower-productivity waters compared to high-productivity regions (Burrows et al., 2014). As in our case, Burrows et al. (2014) assumed that the protein-like group is composed of a fraction of polysaccharides. Consequently, proteins have the same global distribution and seasonal characteristics as polysaccharides. Finally, the lipid-like mixture in Ogunro et al. (2015) also represents a larger group. In addition, the calculations to estimate this macromolecule include the zooplankton levels and the rate of phytoplankton disruption by zooplankton grazing. As a consequence,

higher values for the concentration at the sea surface are found for this group (about 5-fold) compared to  $\text{PL}_{\text{sw}}$  in the present study. Nonetheless, the ocean distribution of  $\text{PL}_{\text{sw}}$  agrees reasonably well with that presented by Burrows et al. (2014). Regardless of the considerations assumed to compute the biomolecules in the ocean, our approach adequately depicts the abundance of the biomolecules in the ocean that are relevant for the aerosols. The seasonal patterns modelled here also agree with those in Burrows et al. (2014), and the polysaccharide group is most frequently represented, followed by amino acids and lipids.

## 5.2 Aerosol organic mass fraction

The organic mass fraction in aerosols depends on the distribution of marine biomolecule concentration in the ocean (Fig. 4d–f). In contrast to the abundance of organic groups in seawater, the OMF of polar lipids is significantly higher than that of the other groups during the hemispheric summer (see Fig. B2). Contributions can be as high as 0.44. In contrast, for  $\text{PCHO}_{\text{aer}}$  and  $\text{DCAA}_{\text{aer}}$ , OMF values are low, reaching a maximum of 0.004 and 0.02, respectively (Fig. 4d–f). The disproportional enrichment observed in the aerosol phase is explained by the aforementioned characteristics of the surface affinity of the main biomolecule groups in seawater (Sect. 2.1). Lipids are highly active surfactants whose surface affinity favours their transfer to the aerosol phase. Consequently, the OMF of  $\text{PL}_{\text{aer}}$  is 2 to 3 orders of magnitude greater than that of  $\text{PCHO}_{\text{aer}}$  and  $\text{DCAA}_{\text{aer}}$  (Fig. 4d, e), and these high values persist globally.

Among the biomolecules,  $\text{PL}_{\text{aer}}$  OMF is the group showing the most pronounced seasonal patterns with values generally decreasing towards the Equator during the hemispheric summer (Table 7 and Fig. B2c, f, j, m).  $\text{PCHO}_{\text{aer}}$  and  $\text{DCAA}_{\text{aer}}$  OMF values, on the other hand, remain uniform across seasons for subtropical and equatorial areas (see Fig. B2). For the polar regions, the abundance of all organic groups in aerosols has a clear seasonality, with strong changes for the  $\text{PL}_{\text{aer}}$  group (see Fig. B2d–j). These seasonal characteristics are caused by an increase in marine primary production as light limitation decreases at the end of the winter. With melting sea ice, light is available in ice-free areas or passes through the thin ice triggering the photosynthesis of phytoplankton. Once nutrients present in seawater are consumed and the polar night sets in, the biological productivity and atmospheric contribution of marine organics are significantly diminished, especially for  $\text{PL}_{\text{aer}}$ .

As expected, the responses of the various groups mirror those in Burrows et al. (2014). Nevertheless, based on the fundamental distinctions among the organic classes analysed, between the two studies, our OMF values are comparatively smaller yet still comparable to their findings.

**Table 6.** Carbon concentration of marine biomolecules for December–January–February (DJF) and June–July–August (JJA) as a multiannual monthly mean for the period 1990–2019 averaged over the polar regions (Arctic Ocean 60–90° N, Southern Ocean 60–90° S), northern and southern subtropics (23–60° N and 23–60° S), and Equator (23° N–23° S). Values are in millimoles carbon per cubic metre ( $\text{mmol C m}^{-3}$ ). In parentheses, the multi-seasonal and regional standard deviation.

Regions	PCHO <sub>sw</sub>		DCAA <sub>sw</sub>		PL <sub>sw</sub>	
	JJA	DJF	JJA	DJF	JJA	DJF
Arctic Ocean	2.43 (1.20)	> 0.52 (0.22)	0.73 (0.36)	> 0.16 (0.07)	0.57 (0.36)	> $2.4 \times 10^{-6}$
Southern Ocean	0.41 (0.19)	< 3.31 (2.0)	0.13 (0.06)	< 0.99 (0.6)	$1.5 \times 10^{-7}$	< 0.31 (0.16)
N. subtropics	4.09 (1.41)	> 2.85 (1.53)	1.22 (0.42)	> 0.85 (0.46)	0.16 (0.13)	> 0.05 (0.05)
S. subtropics	2.21 (1.42)	< 3.81 (1.31)	0.66 (0.43)	< 1.14 (0.4)	0.03 (0.04)	< 0.13 (0.07)
Equator	5.97 (0.71)	≈ 6.0 (0.63)	1.78 (0.21)	≈ 1.79 (0.19)	0.11 (0.03)	= 0.11 (0.03)

**Table 7.** OMF of biomolecule groups in aerosols for the same regions and seasons in Table 6.

Regions	PCHO <sub>aer</sub>		DCAA <sub>aer</sub>		PL <sub>aer</sub>	
	JJA	DJF	JJA	DJF	JJA	DJF
Arctic Ocean	0.001 (0.001)	> 0.0004 (0.0002)	0.006 (0.002)	> 0.002 (0.001)	0.31 (0.09)	> $3.35 \times 10^{-6}$
Southern Ocean	0.0003 (0.0001)	< 0.002 (0.001)	0.001 (0.001)	< 0.009 (0.005)	$2.2 \times 10^{-7}$	< 0.24 (0.081)
N. subtropics	0.003 (0.001)	> 0.002 (0.001)	0.013 (0.004)	> 0.01 (0.005)	0.158 (0.051)	> 0.059 (0.049)
S. subtropics	0.002 (0.001)	< 0.003 (0.001)	0.008 (0.005)	< 0.012 (0.004)	0.039 (0.044)	< 0.134 (0.047)
Equator	0.004 (0.0004)	= 0.004 (0.0004)	0.019 (0.002)	= 0.019 (0.002)	0.124 (0.026)	≈ 0.126 (0.025)

### 5.3 Evaluation of modelled biomolecules at the ocean surface

A comparison of simulated biomolecule concentrations with their measured counterparts in seawater is presented in this section. Each group is analysed against its analogous group from observations (see Sect. 4.1), supported by a discussion of the factors associated with model uncertainties. Figure 5 shows the ocean concentration of modelled and observed quantities for the locations in Fig. 2 for which ocean measurements were available (Table 5). Note that modelled PCHO<sub>sw</sub> and semi-labile DCAA<sub>sw</sub> represent a fraction of measured DCCHO<sub>sw</sub> and DCAA<sub>sw</sub>, whereas observed PG<sub>sw</sub> forms part of the PL<sub>sw</sub> group.

#### 5.3.1 Carbohydrates

The model (coral boxes in Fig. 5) can capture most of the regional variations seen in observations (blue boxes in Fig. 5). Quantities tend to be higher for the North Atlantic Ocean (NAO) compared to the Western Antarctica Peninsula (WAP). The lowest PCHO<sub>sw</sub> concentration occurs at the southern station. This may be attributable to nutrient iron limitation in the Antarctic region (Gürses et al., 2023). Interestingly, the variability for WAP is better represented, although at a higher value than observations. Greater quantities are found at PUR12 and PUR17, where nutrients are transported from the seabed to the surface. Here, the modelled PCHO<sub>sw</sub> concentration is in good agreement with observed DCCHO<sub>sw</sub>, with a modelled median of  $4.1 \pm 0.39$  and

$3.8 \pm 0.16 \text{ mmol C m}^{-3}$  for PUR12 and PUR17, respectively. The lowest normalized mean bias (NMB) is detected for PUR17 ( $-0.08$ ), whereas values are slightly overestimated for WAP (NMB = 0.14) and underestimated for PUR12 (NMB =  $-0.43$ ).

The significant variability observed in PUR12 is not adequately captured by the model. The sampling depth may provide an explanation for this. The quantities would likely be greater for PUR12 if the water samples had been collected at 20 cm depth, in contrast to 1–3 m for PUR17. Maßmig and Engel (2021) found that concentrations of DCCHO and DCAA decrease with depth in this region. Note that FESOM2.1–REcoM3 vertical resolution is coarser and cannot resolve the processes within the SML solely including an average of the upper 5 m depth. Additionally, the model data used are a volume-weighted mean over the upper 30 m, and it is unlikely that subsurface water biomolecule abundances are accurately represented. Nonetheless, our results indicate that the modelled surface carbon concentrations of the biomolecules are in reasonably good agreement with the observations.

On the other hand, the modelled concentrations are about 4 times higher than the measurements for NAO ( $5.75 \pm 2.48 \text{ mmol C m}^{-3}$ ) and 2.5 times higher for CVAO ( $6.12 \pm 0.01 \text{ mmol C m}^{-3}$ ). NMB values for these locations are 2.24 and 1.38 for the northern and tropical sites, respectively. For these sites, the sampling size is relatively small ( $n = 3$ ) and the observations may not fully represent DCCHO<sub>sw</sub> in the region. Nevertheless, the overestimation by

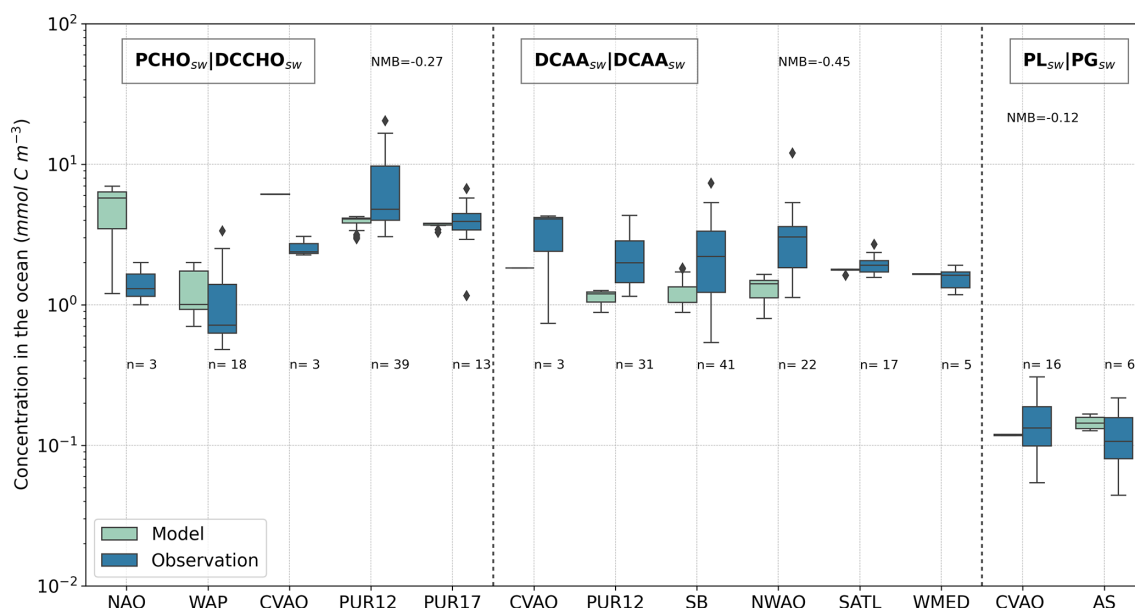


**Figure 5.** Box plot of carbon concentration in seawater of modelled  $\text{PCHO}_{\text{sw}}$ ,  $\text{DCAA}_{\text{sw}}$ , and  $\text{PL}_{\text{sw}}$  and measured  $\text{DCCHO}_{\text{sw}}$ ,  $\text{DCAA}_{\text{sw}}$ , and  $\text{PG}_{\text{sw}}$  for the locations in Fig. 2 (see also Tables 2 and 4 for the compounds and location abbreviations, respectively). Blue boxes represent the bulk water samples (Table 5), and coral boxes are the modelled biomolecule concentration interpolated to the coordinates where the water samples were collected. Normalized mean bias (NMB) is included for each group; number of observations ( $n$ ) is included for all sites. The formula to calculate NMB may be found in Table A1.

the model could be explained by the carbon-overflow hypothesis (Engel et al., 2004, 2020), which states that carbon exudation is increased under nitrogen-limiting conditions. Moreover, bacteria are abundant in oligotrophic provinces like at CVAO and likely consume DOC, a process that is not explicitly represented in FESOM2.1–REcoM3 (Gürses et al., 2023).

In addition to the factors mentioned, we also link the overestimation in polar regions to the fixed fraction of exuded DOC that is generalized to all phytoplankton growth phases. Phytoplankton acidic polysaccharide excretion tends to be stronger during the post-bloom period compared to the phytoplankton growth phase. The amount of  $\text{PCHO}_{\text{sw}}$  exuded could be half of that currently used in the model representative of the post-bloom phase (Schartau et al., 2007).

### 5.3.2 Amino acids

For DCAA, the computed quantities are within the same range for all stations. Western Mediterranean (WMED) and subtropical Atlantic (SATL) are properly represented with median values close to observations ( $1.66 \pm 0.01$  and  $1.78 \pm 0.05 \text{ mmol C m}^{-3}$ , respectively) and a low model bias (NMB = 0.07 and  $-0.09$ , respectively). The oligotrophic sites show significantly less variability during the sampling period (September to October). However, they also have fewer data samples compared to other stations. Pertaining to the other locations, the estimated concentrations are confined to the lower quartile of the observations. The mea-

sured levels for PUR12, Stony Brook (SB), and the northwest Atlantic Ocean site (NWAO) are closely aligned. Among them, Stony Brook has the widest range in the sampled  $\text{DCAA}_{\text{sw}}$ . The higher variability is attributed to a substantial number of year-round measurements conducted at this location. For these subtropical sites, the variability is also apparent in the modelled  $\text{DCAA}_{\text{sw}}$ ; however, it is not properly captured. The normalized model bias ranges between  $-0.6$  and  $-0.49$  for these stations, indicating an underestimation of the observed values. Nonetheless, apparent regional patterns are also found in the simulated biomolecules. For example, as for the observations, CVAO has the largest values and median concentrations of modelled  $\text{DCAA}_{\text{sw}}$ . Similarly, for NWAO ( $1.4 \pm 0.28 \text{ mmol C m}^{-3}$ )  $\text{DCAA}_{\text{sw}}$  tends to be higher than for PUR12 ( $1.2 \pm 0.12 \text{ mmol C m}^{-3}$ ) and SB ( $1.04 \pm 0.29 \text{ mmol C m}^{-3}$ ).

The differences between the modelled and measured values are determined primarily by the approach used to calculate  $\text{DCAA}_{\text{sw}}$ . This biomolecule group was derived from the  $\text{PCHO}_{\text{sw}}$  concentration. Hence, detailed processes relevant for the production of amino acids in seawater are not represented here. Furthermore, as for carbohydrates, the concentrations of  $\text{DCAA}_{\text{sw}}$  tend to be greater near the surface (Maßmig and Engel, 2021). Therefore, the underestimations found for most cases could also be determined by the subsurface sampling depth, which was a maximum of 30 cm. Despite this, the modelled quantities agree reasonably well with the observed  $\text{DCAA}_{\text{sw}}$ .

### 5.3.3 Polar lipids

The observed  $PG_{sw}$  concentrations for the Adriatic Sea (AS) are slightly lower than for CVAO. In contrast, our results show higher concentrations for AS ( $0.14 \pm 0.02 \text{ mmol C m}^{-3}$ ) than for CVAO ( $0.12 \text{ mmol C m}^{-3}$ ). Note that  $PG_{sw}$  may not fully represent all polar lipids in seawater. Nevertheless, the model values are in good agreement with the observed  $PG_{sw}$ , with the lowest model biases (NMB =  $-0.12$ ) compared to the other groups.

The observations indicate that the presence of the  $PG_{sw}$  group exhibits a strong correlation with the presence of phytoplankton (Triesch et al., 2021b). Therefore, the model estimates are closely aligned with the observed fraction of lipids produced by phytoplankton excretion. Nevertheless, the model cannot reproduce the variability for the tropical station. The monthly median values for this case remain within the same range ( $0.11 \pm 0.03 \text{ mmol C m}^{-3}$  in September and  $0.15 \pm 0.1 \text{ mmol C m}^{-3}$  in October); however, there are notable inter-month changes that cannot be captured by the monthly means of the model.

Despite the fact that each biomolecule is analysed against broader measured groups in the ocean, this comparison serves as an indication of how effectively the modelled biomolecules are represented in terms of magnitude and geographic distribution.

In summary, model uncertainties depend on the considerations used to compute biomolecules, in which we neglected processes involved in their production or consumption. Additionally, the temporal and spatial resolution of the model is a source of uncertainty. Firstly, the monthly model values cannot represent changes within the same month (e.g. PUR12 and CVAO). Therefore, in certain instances, minor variations within a month may not be discernible, resulting in relatively homogeneous values and minimal standard deviations for the modelled quantities, such as CVAO, SATL, and WMED. Secondly, a common feature for tropics and subtropics is the coarser resolution of the non-uniform FESOM2.1-REcoM3 model mesh (Schourup-Kristensen et al., 2018) which could, to some extent, decrease the model accuracy for those regions. Lastly, the averaged values over the first 30 m of the model output agree better with observed biomolecule groups when the sampling depth was 1 m or deeper. Furthermore, for some stations (e.g. CVAO) the number of water samples was small, often within the same month, and may not be statistically representative of the existent variable conditions of the biomolecules for the region.

Regardless of the model biases, the calculated quantities lay within the same order of magnitude compared to observations for all cases. The different abundances of biomolecule groups in the ocean are well captured. The lipid group is the least abundant, with a concentration at least 1 order of magnitude lower than that of carbohydrates and amino acids.

## 6 Global atmospheric simulations of PMOA

We have already discussed in detail the geographical distribution and seasonality of marine biomolecules. Their concentrations at the sea surface serve as boundary conditions for the aerosol model. The results of the global aerosol simulations are presented in the following sections. We included an analysis of global mean burden and emission mass flux in the context of previous PMOA modelling studies. Furthermore, a comprehensive model evaluation against aerosol measurements is presented.

### 6.1 Emission and transport characteristics

The global mean emission and burden values of marine aerosol are summarized in Table 8 for all organic species and sea salt. In addition, PMOA quantities are given as totals of the marine organic aerosol groups. Global emissions and burden are mainly governed by  $PL_{aer}$ , representing about 1 % of the sea salt emission by mass. This group accounts for 86.7 % of PMOA, whereas  $PCHO_{aer}$  and  $DCAA_{aer}$  make up 2.3 % and 11 %, respectively. Since hygroscopicity parameters are assumed to be identical and all groups are emitted into the same aerosol mode of the HAM model, their contribution to the total burden remains relatively unchanged compared to the emissions.

The global emission values modelled in this study total  $12.1 \text{ Tg yr}^{-1}$ , which is within the range of previous studies that vary between 9 and  $27 \text{ Tg yr}^{-1}$  (Meskhidze et al., 2011; Huang et al., 2018; Zhao et al., 2021). Similarly, a total mean burden of  $0.075 \text{ Tg}$  agrees with other studies, ranging from 0.048 to  $0.097 \text{ Tg}$  (Huang et al., 2018; Zhao et al., 2021; Burrows et al., 2022). Given the similarities in terms of model configuration, our values are closer to the results by Huang et al. (2018) despite the chl-*a* approach used in their study to compute PMOA. This indicates that the driving aerosol-climate model has a greater influence on the final computed PMOA emissions than the specific representation of marine organics. There is also likely attributable to the sea salt emission scheme employed within the model. Therefore, the ratio of PMOA to SS emission mass fluxes varies across studies, and in our case, it is larger (1.16 %, Table 8) than the ratios presented by Zhao et al. (2021) (0.67 %) and Meskhidze et al. (2011) (0.7 %).

The PMOA representation depends directly on wind speed (Gantt et al., 2011) or on a sea salt emission source function (Meskhidze et al., 2011; Zhao et al., 2021). Sea salt emissions are typically parameterized in relation to the 10 m wind speed power law and/or as a function of the sea surface temperature (Gong, 2003; Mårtensson et al., 2003; Long et al., 2011).

For a more in-depth understanding of the driving processes that control the emission, dispersion, and removal of marine organic aerosol, we examine the connection among multiple model variables. In our study, the PMOA surface emission

fluxes (Fig. 6a) are mainly driven by surface wind. Their geographic distribution is strongly linked to that of sea salt. Nonetheless, in regions where sea salt emissions are relatively low (e.g. high latitudes over 60° of each hemisphere during summer), the distribution of marine organic aerosol is primarily dominated by the elevated biological activity during the bloom period. The strongest emission fluxes occur in the Indian Ocean followed by the North Pacific Ocean with maximum values of 7.82 and 4.88 ng m<sup>-2</sup> s<sup>-1</sup>, respectively. The total mean emission flux for North Pacific waters tends to be 35 % larger than that for the North Atlantic. For the Southern Ocean, the total emission flux is low (0.14 Tg yr<sup>-1</sup>), and values in neighbouring waters (South Atlantic, Indian, and Pacific oceans) are 7- to 23-fold higher.

Once emitted, aerosols are advected and driven by the general atmospheric circulation. If they are not scavenged by wet deposition mechanisms, they will remain longer in the atmosphere. These processes regulate the total aerosol burden, which also peaks in regions with lower surface emissions (e.g. equatorial Pacific). In regions with high biological productivity, such as the North Atlantic and North Pacific oceans, the main removal mechanism of PMOA is wet deposition, likely due to large-scale precipitation. In both hemispheres, the transport accumulates the aerosol towards the Equator. In addition, the marine aerosols are advected inland, with a significant incidence in coastal regions and over continental regions (e.g. widespread contributions in South America and Australia). Quantities could be as high as 0.3 mg m<sup>-2</sup> and even stronger in the northwest of India and the Horn of Africa.

The burden exhibits a similar behaviour to the emission flux, regarding the occurrence in the oceans. Quantities for the Pacific Ocean (0.017 to 0.019 Tg) remain larger than for the Atlantic Ocean (under 0.0072 Tg). Unlike the Atlantic, the difference in the burden between North Pacific and South Pacific increases and is reversed when compared to the emissions. Such differences, in which the highest emissions do not coincide with greater burdens, are caused by the transformation and transport processes that the aerosols undergo in the model. In the Southern Ocean, for instance, the total burden is at 0.0003 Tg about 50-fold lower than in the Indian Ocean. Lastly, the emissions and burden in the Arctic are among the lowest by approximately 2 and 3 orders of magnitude in comparison to the North Atlantic waters.

## 6.2 Species-wise evaluation

In this section, we present the results of a comprehensive analysis of species-resolved offline-computed OMF and ECHAM6.3–HAM2.3 aerosol concentrations against observations. The modelled aerosol organic mass fraction is the result of applying OCEANFILMS with the ocean biomolecule quantities as input data. As a reminder, the OMF depicts the transition from marine organic material to the aerosol phase for each group, and it is entirely free of meteorolog-

**Table 8.** Global mean emission flux and burden of marine species and sea salt. Note that emissions of PMOA are confined to the accumulation mode, whereas SS emissions occur in both the accumulation and coarse modes.

Species	Emission (Tg yr <sup>-1</sup> )	Burden (Tg)	PMOA/SS emission (%)
PCHO <sub>aer</sub>	0.28	0.0017	0.03
DCAA <sub>aer</sub>	1.33	0.0082	0.13
PL <sub>aer</sub>	10.5	0.065	1.0
Total PMOA	12.1	0.075	1.16
SS	1042	3.76	–

ical influences. In contrast, aerosol concentration is strongly affected by wind stress, which triggers sea salt emission in the aerosol model. Hence, we have included the model evaluation against sea salt aerosol concentration for the stations where observations of marine organics are available (Fig. 7). Sodium amounts from observations were used to calculate sea salt concentrations, as explained in Sect. 4.1.

For comparison with measurements of marine organic aerosols, we account on the sub-micron aerosol concentration and estimated OMF from observations. For evaluating the model aerosol quantities PCHO<sub>aer</sub>, DCAA<sub>aer</sub>, and PL<sub>aer</sub>, measured CCHO<sub>aer</sub>, CAA<sub>aer</sub>, and PG<sub>aer</sub> were selected accordingly. In addition, measured organic mass (OM) concentrations are compared with the modelled total PMOA. Simulated and observed quantities for various stations were compiled into a multi-panel box plot in Fig. 8. A detailed description of the observational data and the discussion of our model results for each group is provided further below.

### 6.2.1 Sea salt

Owing to the linear relation between marine organic and sea salt aerosol emission mass flux (Eq. 10), the sea salt representation is essential to better understand the origin of model deviations in the analysis of the organic groups. Figure 7 illustrates the interpolated sub-micron SS concentration (gray boxes) in contrast to observations (black boxes). Observed quantities range between 0.06 and 1 μg m<sup>-3</sup>. Modelled results, extend beyond this range, spanning 10<sup>-3</sup> to 2 μg m<sup>-3</sup>. Simulated values tend to underestimate the SS concentration for both northern and southern stations, whereas for the tropical location in Cape Verde (CVAO), simulations are larger than the observed amounts. The strongest negative normalized mean bias (NMB) occurs for the Western Antarctica Peninsula (WAP) followed by Svalbard (SVD) station with an underestimation of the median SS concentration of about 1 order of magnitude.

For the North Atlantic Ocean (NAO), observed sea salt (SS) concentrations lie within the modelled range and exhibit the lowest NMB. Because SS emissions depend on open-ocean conditions, for the polar stations (WAP, SVD,

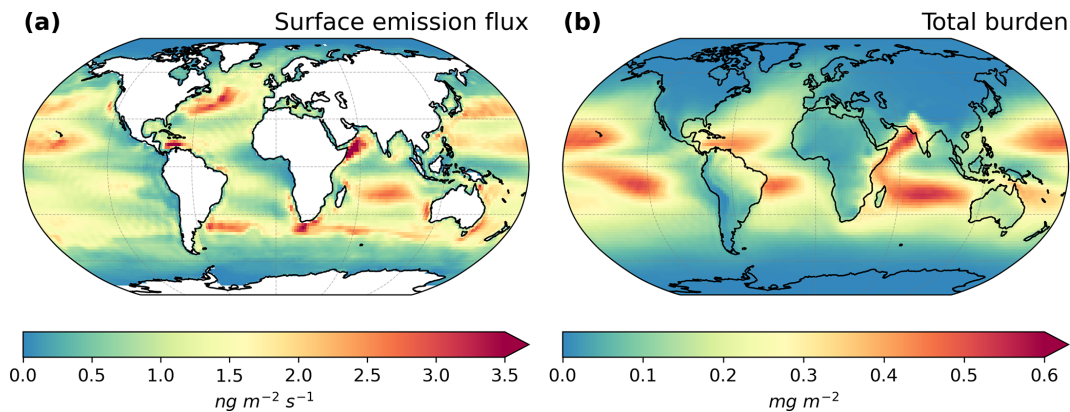


**Figure 6.** Maps of PMOA means of (a) global surface emission mass flux and (b) total burden for the simulated ECHAM6.3–HAM2.3 period 2009–2019.

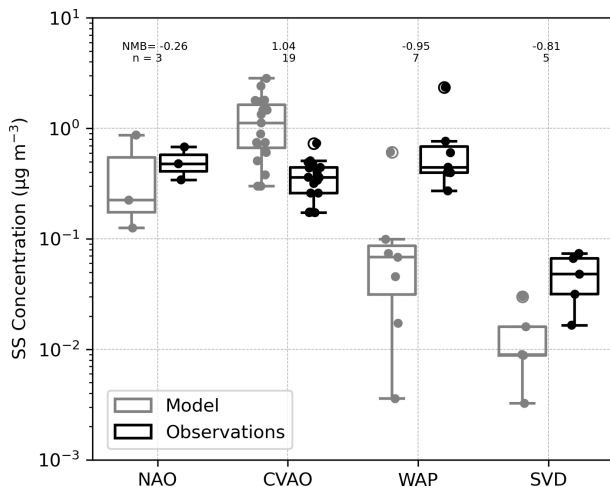


**Figure 7.** Box plot of observed versus ECHAM6.3–HAM2.3-simulated sub-micron sea salt concentration for the stations in Fig. 2 (see also Tables 2 and 4 for the location abbreviations and Table 5 for detailed information regarding the measurement data). Normalized mean bias (NMB) and sample size of observations are given for each station.

and NAO to some extent), the representation of sea ice cover, which is challenging in climate models, will strongly affect the SS emission compared to other ice-free oceanic regions. Additionally, the underestimation at WAP is supported by similar findings in the Southern Ocean by Regayre et al. (2020), who showed that only by tripling the simulated SS concentrations, obtained with the Gong (2003) source function, could the model align with observations. On the other hand, at CVAO, observed SS concentrations fall below the model's first quartile. The elevated sea salt concentrations are likely driven by an excessively high mass emission flux, and ultimately, they may also be associated with inefficient wet deposition, a factor that could be especially significant in tropical regions.

A limitation that applies to the evaluation analysis of all aerosol species is that, as in other global aerosol–climate models, the turbulent transport and boundary layer height are parameterized. Therefore, variable wind conditions over height and time that influence the aerosol detection (measurement heights of less than 60 m) cannot be explicitly resolved by our model.

Large uncertainties persist in modelling sea spray aerosols within climate models (Grythe et al., 2014; Lapere et al., 2023), and regional models have shown varying performance of sea salt source functions among different stations (Barthel et al., 2019). Nevertheless, for the group of stations considered in this study, as well as for other locations worldwide (Tegen et al., 2019), the standard SS emission configuration in ECHAM6.3–HAM2.3 provides the most reasonable representation among the available schemes. Although the resulting biases in SS concentrations affect the predicted PMOA values, the evaluation of marine organics discussed in the following sections remains meaningful and valid despite the discrepancies in SS observations.

## 6.2.2 Carbohydrates

The organic mass fraction of  $\text{PCHO}_{\text{aer}}$  in nascent aerosols obtained from the offline calculation (coral boxes in Fig. 8) is comparatively higher at the tropical station (CVAO) with respect to NAO and WAP. In contrast, measured combined carbohydrates ( $\text{CCHO}_{\text{aer}}$ ) (blue boxes in Fig. 8) are within the same range for all stations. For CVAO, the OMF median value is greater than the observed  $\text{CCHO}_{\text{aer}}$ . Conversely, an underestimation is seen for NAO. The discrepancies are significant for WAP with a negative mean model bias of  $-0.002$ , whereas for NAO and CVAO, OMF is within the same order of magnitude of observations.

Similarly, the simulated concentrations (light pink in Fig. 8) are lower than the observations (dark pink boxes in Fig. 8) for high-latitude sites. As a result, the aerosol concentrations are also underestimated for NAO and WAP,

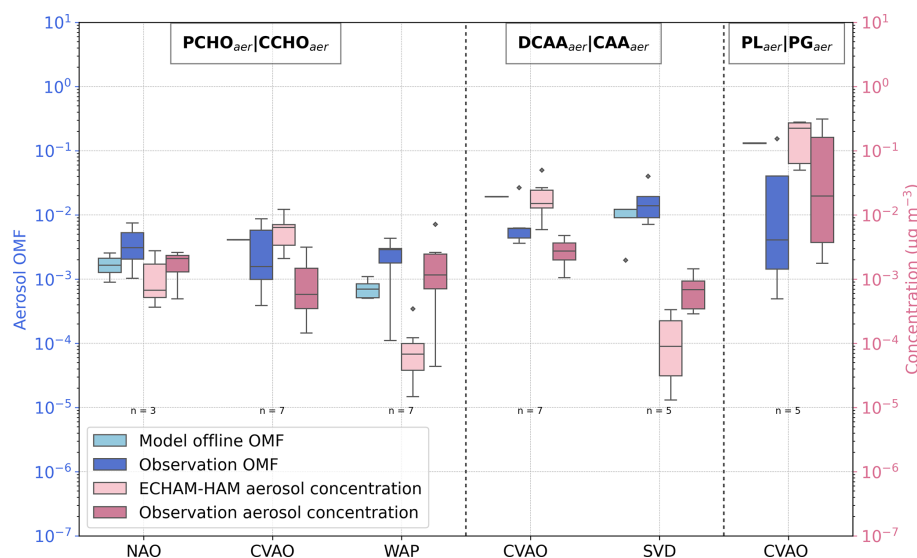


**Figure 8.** Box plot of the species-resolved, offline-computed OMF and ECHAM6.3–HAM2.3-simulated concentrations in contrast to the measured values. Sub-micron aerosols  $\text{PCHO}_{\text{aer}}$ ,  $\text{DCAA}_{\text{aer}}$ , and  $\text{PL}_{\text{aer}}$  are compared to  $\text{CCHO}_{\text{aer}}$ ,  $\text{CAA}_{\text{aer}}$ , and  $\text{PG}_{\text{aer}}$ , respectively, for the stations in Fig. 2 (see also Tables 2 and 4 for the compounds and location abbreviations, and Table 5 for detailed information regarding the measurement data). Dashed lines separate each group, and the name tags indicate the modelled marine aerosols separated by a straight bar from the measured aerosol components selected for the evaluation. Coral and light pink colours mark modelled values, whereas blue and dark pink indicate observations of OMF and aerosol concentration (in  $\mu\text{g m}^{-3}$ ), respectively. The sample size of observations ( $n$ ) is included for all sites.

while higher values than the observations were modelled for CVAO. It is likely that the slight overestimation for CVAO is due to the relatively higher concentration of this biomolecule in seawater. Interestingly, there is no similar response for NAO or WAP for which the ocean biomolecules were over-represented by the model or in good agreement with the water samples. Possible causes for this contradicting pattern can be explained as follows.

Firstly, for NAO and WAP, aerosols were sampled while the ship was in motion. Therefore, aerosol samples were influenced by a much higher number of ocean areas than could be covered by surface seawater sampling. Secondly, relevant processes that favour the transfer of carbohydrates to the air are not included in the OCEANFILMS version used in this study. The under-representation of the organic fraction and concentration of carbohydrates in marine aerosols by the model seems to be a limitation of the monolayer Langmuir model, which neglects molecule interactions (Burrows et al., 2014). In addition to the aerosol measurements included in the present work, other studies employing different detection techniques have quantified even higher organic enrichment in aerosols attributed to carbohydrates (Russell et al., 2010; Frossard et al., 2014). Co-adsorption mechanisms facilitate the transfer to the aerosol phase of less surface-active compounds, such as polysaccharides or proteins, which are less enriched at the sea surface microlayer (SML). This occurs when such groups attach to the surfactants already coating

the air bubble due to ionic interactions (Burrows et al., 2016; Hasencz et al., 2019; Link et al., 2019).

Furthermore, given our model assumption,  $\text{PCHO}_{\text{aer}}$  is a fraction of  $\text{CCHO}_{\text{aer}}$ . Therefore, modelled dissolved acidic polysaccharides may not represent the total measured combined carbohydrates group but rather a fraction. Ultimately, given that aerosols are not collected under controlled conditions, concentrations may be affected by newly released polysaccharides by bacteria in the atmosphere (Zeppenfeld et al., 2021, 2023). Hence,  $\text{CCHO}_{\text{aer}}$  concentrations may also originate from secondary sources other than the primary oceanic sea spray emissions.

In addition to the aforementioned factors, the negative normalized mean biases found in the organic aerosol concentration for WAP ( $-0.95$ ) and NAO ( $-0.26$ ) can be associated with an underestimation of the simulated sea salt concentrations (Fig. 7). Sensitivity experiments with the ECHAM6.3–HAM2.3 model performed by Huang et al. (2018) demonstrated that when PMOA is emitted together with sea salt as sea spray, PMOA emissions are particularly sensitive to the sea salt source function selected.

### 6.2.3 Amino acids

The organic mass fractions of combined amino acids ( $\text{CAA}_{\text{aer}}$ ) from measurements (Fig. 8 second panel) remain higher than that for  $\text{CCHO}_{\text{aer}}$ , a pattern that is also reflected in the offline calculated OMF. In contrast to observations, the median value of simulated OMF of  $\text{DCAA}_{\text{aer}}$  is slightly

smaller for Svalbard (SVD) in comparison to CVAO. These OMF values tend to overestimate observations significantly for the tropical station, with a normalized mean bias of 1.19. However, for the northern site, model results are at the lower end of observations with small differences ( $NMB = -0.46$ ).

On the other hand, despite the OMF data from measurements in SVD remaining larger than that in CVAO, the opposite occurs for the aerosol concentration. The dissimilarities are explained by the higher mean sodium concentration in CVAO (Fig. 7), which compensates for the high occurrence of  $CAA_{aer}$ . The model nicely captures such regional characteristics for these stations. The concentration simulated at CVAO has a positive bias of  $0.02 \mu\text{g m}^{-3}$  that is amplified as sea salt is overestimated in our model for this site (Fig. 7 with a bias of  $0.7 \mu\text{g m}^{-3}$  for the SS sampled during the  $CAA_{aer}$  observations).

For the measurement campaign on Svalbard, the model bias is negative ( $-6 \times 10^{-4} \mu\text{g m}^{-3}$ ) and the median concentration is about 10-fold smaller than the observations. This may be related to the low sea salt content (SVD in Fig. 7), which we consider a determinant for the low  $DCAA_{aer}$  aerosol concentrations in the model.

#### 6.2.4 Polar lipids

The scarce measurements of lipid aerosol within the simulated period limit our comparison to only the location of CVAO (Fig. 8 third panel). For this site, the measured concentrations and OMF exhibit significant disparities for  $PG_{aer}$  when compared to  $PCHO_{aer}$  and  $DCAA_{aer}$ . However, the model is capable of accurately representing the higher concentration of lipids in aerosols. Simulated OMF of  $PL_{aer}$  accounts for up to 84 % of total OMF for CVAO, whereas that of  $DCAA_{aer}$  and  $PCHO_{aer}$  is less than the 13 % and 3 %, respectively. As for van Pinxteren et al. (2023), we found that the lipids group has the highest contributions to the total marine organic aerosols.

Observations of  $PG_{aer}$  are widely spread, with a large interquartile range. The OMF values from measurements range between  $4.9 \times 10^{-4}$  and  $1.5 \times 10^{-1}$ , whereas the aerosol concentration goes from  $1.8 \times 10^{-3}$  to  $3.1 \times 10^{-1} \mu\text{g m}^{-3}$ . In contrast, simulated values do not present such variability. Modelled OMF lays at the upper end of values calculated from measurements ( $1.3 \times 10^{-1}$ ) with a mean bias of 0.09. Similarly, the aerosol concentration is also overestimated ( $MB = 0.08 \mu\text{g m}^{-3}$ ).

The  $PL_{aer}$  group may encompass other subgroups rather than  $PG_{aer}$ . This could partially explain the overestimation of aerosol quantities by a factor of 3. However, these discrepancies, as previously mentioned, are strongly influenced by the misrepresentation of sea salt at this tropical station. Furthermore, in addition to the sea–air transfer via bubble bursting, there are other processes that influence the lipid concentration in aerosols. For instance, the presence of bacteria in ma-

rine aerosol particles could lead to atmospheric lipid production and degradation (Triesch et al., 2021b).

#### 6.2.5 Total organic matter

Finally, to understand the contribution of marine aerosols (PMOA) to total organic matter given the background OC concentration, we examine the modelled organic concentration against observed  $OM_{aer}$  in sub-micron aerosol (Fig. 9). As previously introduced, OC originates from anthropogenic sources or biomass burning in the model. In contrast, simulated PMOA is the unique marine source to the aerosol organic matter.

The observed aerosol concentrations are highest for CVAO and NAO (dark pink boxes in Fig. 9). For the Antarctica station (WAP), quantities are approximately 1 order of magnitude smaller compared to the other sites. Simulated OC (Fig. 9a) tends to slightly overestimate the observed organic matter concentration for NAO and CVAO, being more pronounced for the northernmost location. At the tropical site, modelled values are within the same range as observations, whereas for NAO, values concentrate at the upper end of measured quantities. Lastly, WAP is the only area in which organic matter is poorly represented when the local marine aerosols are not considered.

Note that the assumptions introduced here to calculate the  $OM_{aer}$  are based on measured OC, which can be variable, and are thus a source of error. What is more important here, however, is the fact that the sites in the northern and subtropical Atlantic are strongly affected by anthropogenic and biomass burning sources, which actually dominate and can lead to high levels of organic carbon. In accordance with the results of the detailed evaluation by Tegen et al. (2019), the non-marine contributions in both regions can vary considerably in ECHAM6.3–HAM2.3. Based on this, we consider the overestimations of OC at NAO and CVAO to be likely related to uncertainties in biomass burning aerosol emissions, whose representation remains challenging for aerosol–climate models.

As a result of accounting for PMOA as an additional source of organic aerosols (Fig. 9b) the total simulated concentration increases at NAO and CVAO leading to a rise in model biases and errors. Conversely, a notable improvement is observed in the more pristine region in the Southern Ocean (WAP) where the absolute mean bias and normalized mean bias decreased by approximately 21 % to 29 % when considering PMOA. Overall, across the three stations, the correlation between modelled and observed organic matter remains moderate, with little change upon incorporating PMOA (decreasing slightly from 0.61 for OC to 0.57 for OC + PMOA). Nevertheless, this analysis highlights the quantifiable relevance of PMOA and its significant contribution to organic aerosol mass in remote oceanic regions.

Despite the overall uncertainties and model biases in representing the organic fraction and aerosol concentrations for

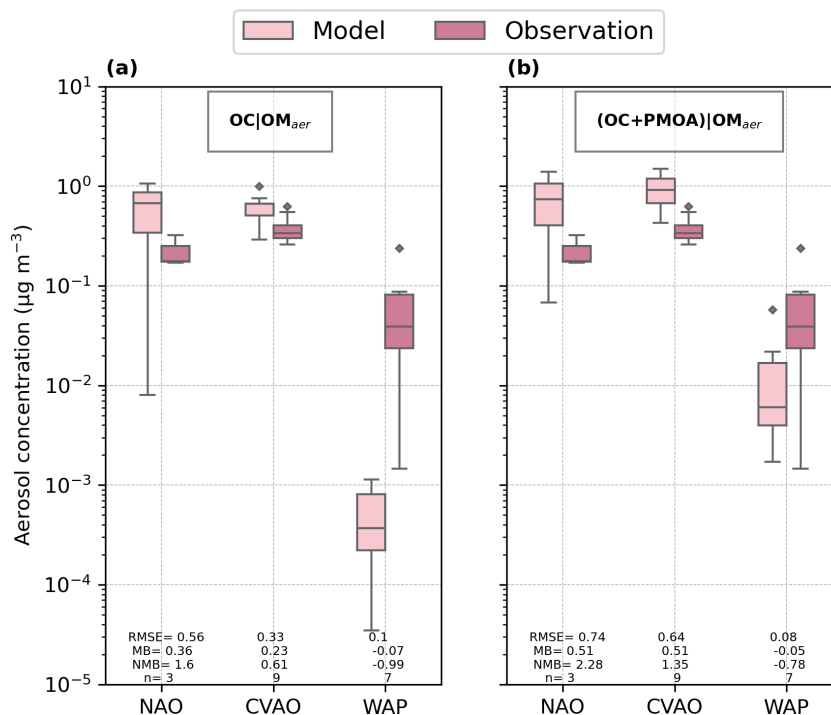


**Figure 9.** Box plot of the ECHAM6.3–HAM2.3-simulated sub-micron aerosol OC and (PMOA+OC) in contrast to measured  $OM_{aer}$  for the stations in Fig. 2 (see also Tables 2 and 4 for the compounds and location abbreviations, and Table 5 for detailed information regarding the measurement data). The modelled aerosol quantity is separated by a straight bar from the measured aerosol components selected for the evaluation. Root mean square error (RMSE) and the mean bias (MB) (in units of  $\mu\text{g m}^{-3}$ ), the normalized mean bias (NMB), and sample size ( $n$ ) are given for each station (see Table A1 for formulas to calculate the statistical indexes).

point locations, the modelled values range in the same order of magnitude as the observations for most stations. Furthermore, our model can still capture the differential aerosol enrichment of the biomolecule groups also visible in measurements, in which  $PL_{aer}$  predominates in the aerosols with contributions of up to 2 orders of magnitude greater than  $PCHO_{aer}$  and  $DCAA_{aer}$ .

### 6.3 Comparison of PMOA with in situ aircraft measurements

In order to show the capability of the model to represent PMOA in remote oceanic regions, where ground-based measurements are barely feasible or species-resolved quantities are unavailable, we compare the simulated PMOA concentrations with organic aerosol mass from ATom aircraft observations. The comparison in Fig. 10 clearly shows how the model performance improves when PMOA is considered in contrast to the configuration without. For the SPMOAoff case, the concentration of the OC tracer is compared, while for the SPMOAon simulation it is the total OC and PMOA. Note that modelled OC only comprises emissions from anthropogenic sources and biomass burning.

Overall, the correlation with observations is high for both experiments. However, a notable underestimation is ob-

served for the SPMOAoff case, specially for the South Pacific. Model values increase toward a better agreement when PMOA is added and the correlation coefficient rises from 0.67 to 0.74 with a significant improvement for several sites. The independent model biases per region indicate that the model biases are considerably reduced for the South Pacific and Atlantic oceans. Interestingly, adding PMOA leads to an overestimation of the modelled organic aerosols in the central Pacific. This is surprising, since the aerosol load in this region is expected to be governed by local sources. Possibly, the uncertainties in OC emission sources could explain this, as long-range-transported aerosols from the Asian and Australian continents might be the origin of the initially elevated OC aerosol concentrations in this region.

These results are in accordance with a previous study by Pai et al. (2020), who found a strong influence of primary marine organic aerosols of the remote marine boundary layer. Their model simulations, however, tend to overestimate the observed values, with larger biases than in this study. This might be the result of the differences in the marine aerosol emission parameterization (using Gantt et al., 2015), and further atmospheric transformation processes are taken into account.

Note that measured organic aerosols (OAs) from ATom aircraft data encompass multiple aerosol sources and types.

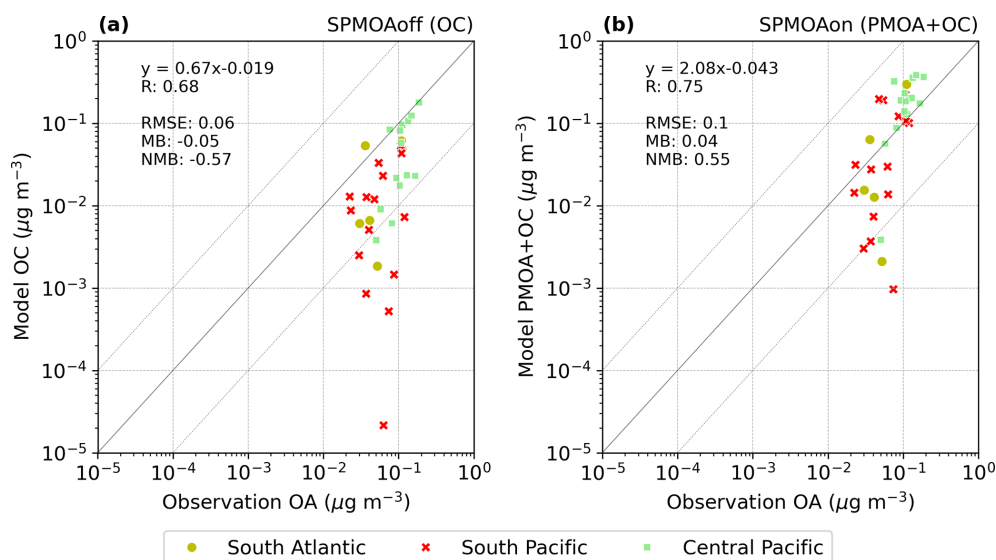


**Figure 10.** Scatter plot of the comparison of aerosol concentration daily averages of ECHAM6.3–HAM2.3-simulated PMOA and organic aerosol aircraft observations (ATom data) for the (a) SPMOAoff and (b) SPMOAon experiments. The data were grouped per region as in Fig. 3. Observed and measured quantities represent the concentration at standard temperature and pressure conditions (273 K, 1 atm). Root mean square error (RMSE) and the mean bias (MB) (in units of  $\mu\text{g m}^{-3}$ ), the normalized mean bias (NMB), the correlation coefficient ( $R$ ), and sample size are given for each station. The formulas to calculate the statistical indexes may be found in Table A1.

The OA includes primary and secondary organic aerosol particles (Hodzic et al., 2020) which could not be disentangled from the original dataset. In our model simulations, only primary aerosols are considered, so the secondary aerosol formation resulting from chemical transformation of the respective precursor species is missing in the comparison on the modelling side. Nonetheless, our findings suggest that by adding PMOA to primary non-marine OC, the model estimates are already significantly improved for southern oceanic regions.

Lastly, the model coarse temporal and spatial resolution is a major source of uncertainties for this comparison. The large daily standard deviation in measured OA indicates the strong variability in the data, which, given our model limitation, cannot be captured. Nonetheless, our results show that by including PMOA, our model represents better the organic aerosol in the lower atmosphere of remote southern oceanic regions. Moreover, seasonal variability, which was not considered here, seems to be a critical factor when validating aerosol model results with ATom data (Gao et al., 2022).

## 7 Summary and conclusions

In this study, primary marine organic aerosols are included in the global aerosol–climate model ECHAM6.3–HAM2.3 to investigate their emission characteristics and distribution. The representation of organic mass fraction is based on the marine emission scheme OCEANFILMS by Burrows et al. (2014). We account for the contribution of three main

marine biomolecule groups in the ocean relevant for the aerosol phase (dissolved acidic polysaccharides ( $\text{PCHO}_{\text{sw}}$ ), dissolved combined amino acids ( $\text{DCAA}_{\text{sw}}$ ), and polar lipids ( $\text{PL}_{\text{sw}}$ )). Marine quantities are based on phytoplankton-exuded carbon calculated by the ocean biogeochemistry model FESOM2.1–REcoM3 and serve as bottom boundary condition to the atmospheric model.

The simulated  $\text{PCHO}_{\text{sw}}$  is the most abundant group in seawater, followed by  $\text{DCAA}_{\text{sw}}$  and  $\text{PL}_{\text{sw}}$ , both of which exhibit lower contributions to the extracellular dissolved organic carbon. The abundance and amounts of molecules are well represented in the simulations compared to worldwide in situ seawater measurements.

The individual marine groups show a diverse global distribution.  $\text{PL}_{\text{sw}}$  ocean concentrations are generally higher in biologically active regions, whereas  $\text{PCHO}_{\text{sw}}$  and  $\text{DCAA}_{\text{sw}}$  groups predominate in subtropical and tropical waters. The distribution of the organic mass fraction of aerosols closely resembles that of the concentrations of biomolecules in oceans. Nevertheless, a differential enrichment in the aerosols was detected. Given the high air–water surface affinity of lipids, this group dominates the organic mass in aerosols, while  $\text{PCHO}_{\text{aer}}$  and  $\text{DCAA}_{\text{aer}}$  tend to be significantly lower in magnitude.

The seasonal patterns of the marine biomolecule and organic aerosol mass fraction were additionally examined. For polar regions, seasonality is remarkable in contrast to mid- and equatorial latitudes. The greatest contribution of the three organic groups occurs during summer in each hemisphere, and the values remain invariant for the Equator. In a

follow-up study, we will comprehensively examine the distinctive characteristics of the Arctic and the evolution of marine biomolecules and PMOA over the past decades, owing to the distinct significance of this region and its prominent alterations in response to changing climate conditions.

The global aerosol model simulations indicate that PMOA emission fluxes are sensitive to multiple factors. Among them, the marine biological activity and surface wind conditions are mainly controlling the occurrence of PMOA. Due to elevated wind speeds, the emission fluxes in the North Atlantic, North Pacific, and Indian waters tend to be stronger. The model estimate of the aggregated PMOA emission globally is  $12.1 \text{ Tg yr}^{-1}$ , corresponding to an atmospheric burden of  $0.075 \text{ Tg}$ .

Furthermore, the modelled mass concentrations of the primary marine organic aerosol were thoroughly evaluated using observations. A comparative analysis of PMOA against organic aerosols from NASA's ATom aircraft campaigns indicated that the model has better correlation for remote Southern Hemisphere oceans when PMOA is included. The species-resolved aerosol evaluation showed that the model could capture the differential organic enrichment in aerosols. Nevertheless, further improvements are needed for the aerosol–climate model. For instance, the underestimation of sea salt emissions affected a more correct representation of the PMOA concentrations. Here, more detailed emission functions of sea salt or sensitivity studies with multiple source functions could lead to better estimates in the future (e.g. Grythe et al., 2014; Albert et al., 2016). Although the uncertainties are large across models and source functions, some improvements in certain regions may be achieved. Moreover, adjusting OCEANFILMS parameters to better characterize the physicochemical properties of the biomolecules studied here could lead to a more accurate representation of the organic fraction in aerosols.

The different emission and transport patterns found in this modelling study suggest that the distinct components of PMOA may exert a differentiated influence on cloud and precipitation formation. Our research provides a model setup that considers diverse marine organic aerosol groups. This model setup will be further developed to incorporate the significance of individual groups or aggregated PMOA in aerosol–cloud interaction processes in future studies. The capability of regional grid refinements for the biogeochemical model provides a vast scope for the approach presented here to compute biomolecules as boundary conditions for a high-resolution aerosol–cloud model simulation. This could be particularly interesting for Arctic studies, as it enables the incorporation of spatial fine structures, such as phytoplankton blooms along marginal ice zones, and evaluate the effect of mixed-phase clouds in the Arctic climate.

## Appendix A: Statistical index formulas

**Table A1.** Formulas of statistic indexes.  $M_i$  and  $O_i$  refer to the model results and observational data  $i$  for each station or region.  $N$  is the data sample size.

Statistics	Formula
Mean bias	$MB = \frac{1}{N} \sum_{i=1}^N (M_i - O_i)$
Normalize mean bias	$NMB = \frac{\sum_{i=1}^N (M_i - O_i)}{\sum_{i=1}^N O_i}$
Root mean square error	$RMSE = \sqrt{\frac{1}{N} \sum_{i=1}^N (M_i - O_i)^2}$

## Appendix B: Maps of monthly biomolecule quantities

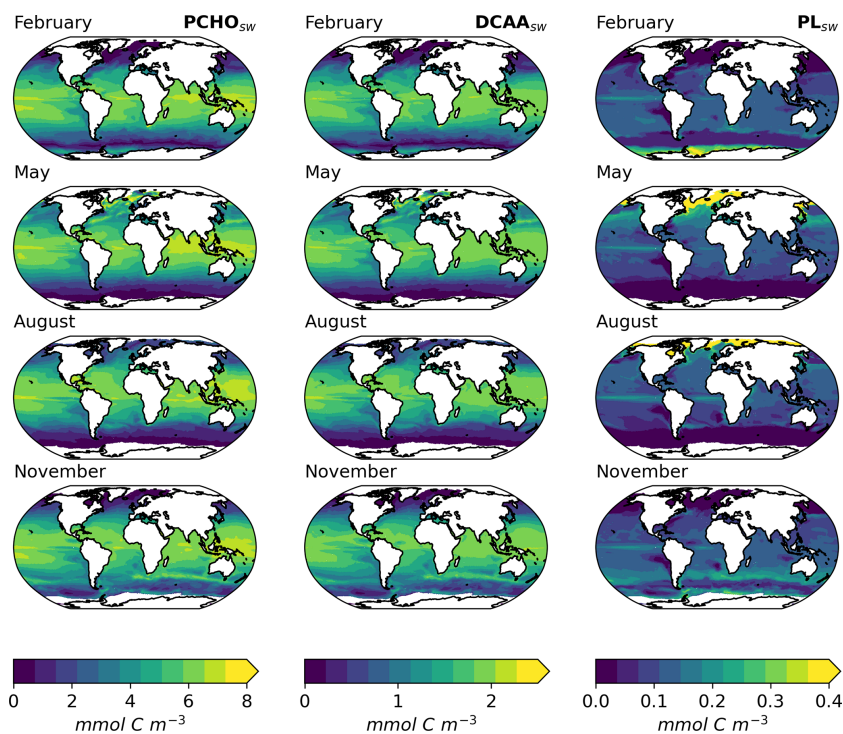


**Figure B1.** Maps of monthly-averaged ocean carbon concentration of  $\text{PCHO}_{\text{sw}}$  (first column),  $\text{DCAA}_{\text{sw}}$  (second column), and  $\text{PL}_{\text{sw}}$  (third column) for February, May, August, and November as a multiannual mean for the period 1990–2019 for sea-ice-free conditions ( $\text{SIC} < 10\%$ ).

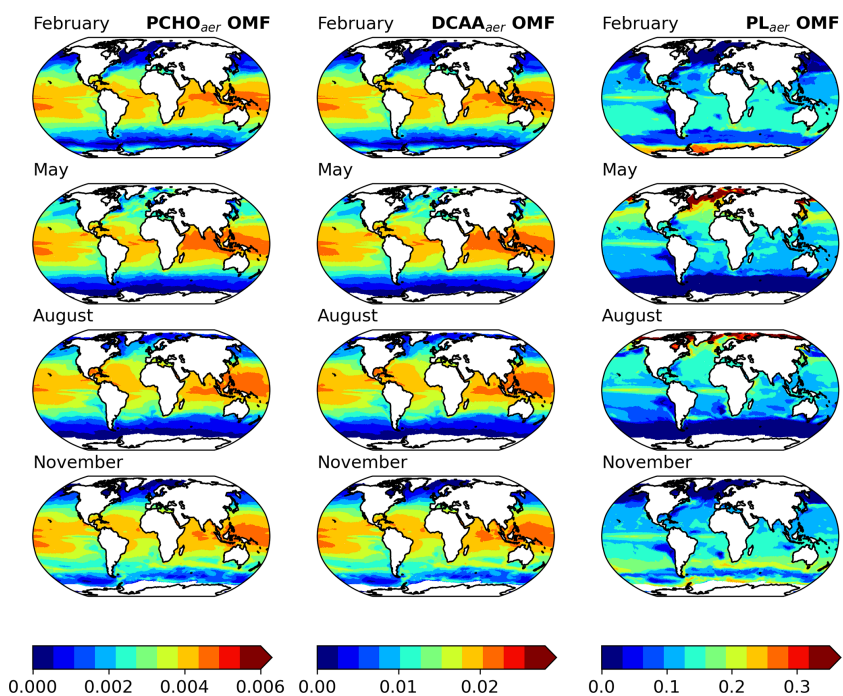


**Figure B2.** Maps of monthly-averaged, offline-computed OMF of  $\text{PCHO}_{\text{aer}}$  (first column),  $\text{DCAA}_{\text{aer}}$  (second column), and  $\text{PL}_{\text{aer}}$  (third column) for February, May, August, and November as a multiannual mean for the period 1990–2019 for sea-ice-free conditions ( $\text{SIC} < 10\%$ ).

**Code and data availability.** The source code of the FESOM2.1–REcoM3 model is available at <https://doi.org/10.5281/zenodo.14017537> (Zeising et al., 2024). The ECHAM–HAM model is accessible to the scientific community under the HAMMOZ Software Licence Agreement, which specifies the terms of use for the model ([https://redmine.hammoz.ethz.ch/projects/hammoz/wiki/1\\_Licensing\\_conditions](https://redmine.hammoz.ethz.ch/projects/hammoz/wiki/1_Licensing_conditions), HAMMOZ, 2024). The model version used in the current study, including the implementation of primary marine organic aerosols’ emission, is archived on Zenodo (<https://doi.org/10.5281/zenodo.14193491>, Leon-Marcos and Heinold, 2024b). Setting files for the simulation experiments and the code of the primary marine aerosol implementation in the model is also documented at <https://doi.org/10.5281/zenodo.14203456> (Leon-Marcos and Heinold, 2024a). The biogeochemistry model tracers to compute the marine biomolecules groups, the ocean biomolecule concentration, and results of the aerosol–climate model simulations are accessible at <https://doi.org/10.5281/zenodo.15172565> (Leon-Marcos et al., 2025). The seawater and aerosol measurement data sets were derived from the referenced literature or requested directly by the authors. The model evaluation with observations was performed with python3 (Python Software Foundation) with available interpolation functions in the module SciPy. In addition, to handle the model data and visualize the results, other python3 libraries such as xarray, pandas, cartopy, and matplotlib were used. Climate Data Operators (CDO) version 2.2.4 was used for adapting the bottom boundary condition data to the ECHAM6.3–HAM2.3 grid and for the posterior interpolation of the aerosol model results to a regular vertical and horizontal grid.

**Author contributions.** ALM developed the approach to compute the biomolecules based on FESOM2.1–REcoM3 model tracers and implemented the marine organic aerosol parameterization in the aerosol model; MZ incorporated the PCHO and TEP as tracers in the biogeochemistry model; MZ and ALM did the post-processing of the ocean data output; ALM and BH planned the aerosol–climate model simulations; ALM performed the models’ evaluation; MvP, SZ, and BH provided scientific advice in the process understanding and model representation of organics abundance in seawater and in aerosol; MvP, SZ, AB, EB, AE, and MF facilitated the access and assisted with most of the data employed for the models’ evaluation; MZ wrote the biogeochemistry model description; ALM wrote the remaining sections of the manuscript draft; MZ, MvP, SZ, AB, EB, AE, MF, IT, and BH reviewed and edited the manuscript; BH supervised and supported the work by providing scientific feedback to all sections; AB, BH, and MvP acquired funding.

**Competing interests.** The contact author has declared that none of the authors has any competing interests.

**Disclaimer.** Publisher’s note: Copernicus Publications remains neutral with regard to jurisdictional claims made in the text, published maps, institutional affiliations, or any other geographical representation in this paper. While Copernicus Publications makes every effort to include appropriate place names, the final responsibility lies with the authors.

**Acknowledgements.** We are grateful for the active and collaborative work among the members within the project “Arctic Amplification: Climate Relevant Atmospheric and Surface Processes, and Feedback Mechanisms” including subprojects B04, C03, and D02. We especially thank the developers of ECHAM–HAM. The ECHAM–HAMMOZ model is developed by a consortium composed of ETH Zürich, Max Planck Institute for Meteorology, Forschungszentrum Jülich, the University of Oxford, the Finnish Meteorological Institute, and the Leibniz Institute for Tropospheric Research and managed by the Centre for Climate Systems modelling (C2SM) at ETH Zürich. The authors are grateful for computing time from the Deutsches Klimarechenzentrum (DKRZ). Computing resources at DKRZ were granted under project number bb1005. The authors express their gratitude for the computing time granted by the Resource Allocation Board and utilized on the supercomputers Lise and Emmy at NHR@ZIB and NHR@Göttingen as a component of the NHR infrastructure. The calculations for this research were conducted with computing resources under the project hbk00084. We are thankful to Susannah Burrows (scientist at Pacific Northwest National Laboratory, Washington, USA) for the assistance provided in the offline implementation of OCEANFILMS and facilitating the ocean macromolecule data from CESM biogeochemical modules for test runs. We thank Christoph Völker (scientist at the Alfred Wegener Institute, Bremerhaven, Germany) for the insightful scientific discussions regarding the biogeochemical processes in the FESOM–REcoM model. We appreciate Svetlana Paul’s (PhD candidate at the Leibniz Institute for Tropospheric Research, Leipzig, Germany) assistance in the implementation and improvement of some post-processing Python tools employed for the model evaluation.

**Financial support.** This research has been supported by the Deutsche Forschungsgemeinschaft (grant no. 268020496) within the Transregional Collaborative Research Centre TRR172.

**Review statement.** This paper was edited by Pearse Buchanan and reviewed by two anonymous referees.

## References

- Abdul-Razzak, H. and Ghan, S. J.: A parameterization of aerosol activation: 2. Multiple aerosol types, *J. Geophys. Res.-Atmos.*, 105, 6837–6844, <https://doi.org/10.1029/1999JD901161>, 2000.
- Al-Hasan, R. H. and Coughlan, S. J.: A method for the determination of glycolic acid in the extracellular products of cultured and natural phytoplankton populations, *J. Exp. Mar. Biol. Ecol.*, 25, 141–149, [https://doi.org/10.1016/0022-0981\(76\)90015-0](https://doi.org/10.1016/0022-0981(76)90015-0), 1976.
- Albert, M., Schaap, M., Manders, A., Scannell, C., O’Dowd, C., and de Leeuw, G.: Uncertainties in the determination of global sub-micron marine organic matter emissions, *Atmos. Environ.*, 57, 289–300, <https://doi.org/10.1016/j.atmosenv.2012.04.009>, 2012.
- Albert, M. F. M. A., Anguelova, M. D., Manders, A. M. M., Schaap, M., and de Leeuw, G.: Parameterization of oceanic whitecap fraction based on satellite observations, *Atmos. Chem. Phys.*, 16, 13725–13751, <https://doi.org/10.5194/acp-16-13725-2016>, 2016.

- Alpert, P. A., Kilthau, W. P., O'Brien, R. E., Moffet, R. C., Gilles, M. K., Wang, B., Laskin, A., Aller, J. Y., and Knopf, D. A.: Ice-nucleating agents in sea spray aerosol identified and quantified with a holistic multimodal freezing model, *Science Advances*, 8, eabq6842, <https://doi.org/10.1126/sciadv.abq6842>, 2022.
- Arnosti, C., Wietz, M., Brinkhoff, T., Hehemann, J.-H., Probandt, D., Zeugner, L., and Amann, R.: The Biogeochemistry of Marine Polysaccharides: Sources, Inventories, and Bacterial Drivers of the Carbohydrate Cycle, *Annu. Rev. Mar. Sci.*, 13, 81–108, <https://doi.org/10.1146/annurev-marine-032020-012810>, 2021.
- Barthel, S., Tegen, I., and Wolke, R.: Do new sea spray aerosol source functions improve the results of a regional aerosol model?, *Atmos. Environ.*, 198, 265–278, <https://doi.org/10.1016/j.atmosenv.2018.10.016>, 2019.
- Biersmith, A. and Benner, R.: Carbohydrates in phytoplankton and freshly produced dissolved organic matter, *Mar. Chem.*, 63, 131–144, [https://doi.org/10.1016/S0304-4203\(98\)00057-7](https://doi.org/10.1016/S0304-4203(98)00057-7), 1998.
- Bigg, E. K. and Leck, C.: The composition of fragments of bubbles bursting at the ocean surface, *J. Geophys. Res.-Atmos.*, 113, D11209, <https://doi.org/10.1029/2007JD009078>, 2008.
- Billmire, E. and Aaronson, S.: The secretion of lipids by the freshwater phytoflagellate *Ochromonas danica*1,2, *Limnol. Oceanogr.*, 21, 138–140, <https://doi.org/10.4319/lo.1976.21.1.0138>, 1976.
- Blanchard, D. C. and Woodcock, A. H.: THE PRODUCTION, CONCENTRATION, AND VERTICAL DISTRIBUTION OF THE SEA-SALT AEROSOL, *Ann. NY Acad. Sci.*, 338, 330–347, <https://doi.org/10.1111/j.1749-6632.1980.tb17130.x>, 1980.
- Burrows, S. M., Hoose, C., Pöschl, U., and Lawrence, M. G.: Ice nuclei in marine air: biogenic particles or dust?, *Atmos. Chem. Phys.*, 13, 245–267, <https://doi.org/10.5194/acp-13-245-2013>, 2013.
- Burrows, S. M., Ogunro, O., Frossard, A. A., Russell, L. M., Rasch, P. J., and Elliott, S. M.: A physically based framework for modeling the organic fractionation of sea spray aerosol from bubble film Langmuir equilibria, *Atmos. Chem. Phys.*, 14, 13601–13629, <https://doi.org/10.5194/acp-14-13601-2014>, 2014.
- Burrows, S. M., Gobrogge, E., Fu, L., Link, K., Elliott, S. M., Wang, H., and Walker, R.: OCEANFILMS-2: Representing coadsorption of saccharides in marine films and potential impacts on modeled marine aerosol chemistry, *Geophys. Res. Lett.*, 43, 8306–8313, <https://doi.org/10.1002/2016GL069070>, 2016.
- Burrows, S. M., Easter, R. C., Liu, X., Ma, P.-L., Wang, H., Elliott, S. M., Singh, B., Zhang, K., and Rasch, P. J.: OCEANFILMS (Organic Compounds from Ecosystems to Aerosols: Natural Films and Interfaces via Langmuir Molecular Surfactants) sea spray organic aerosol emissions – implementation in a global climate model and impacts on clouds, *Atmos. Chem. Phys.*, 22, 5223–5251, <https://doi.org/10.5194/acp-22-5223-2022>, 2022.
- Carlson, C. A.: Production and Removal Processes, Elsevier, 91–151, <https://doi.org/10.1016/B978-012323841-2/50006-3>, 2002.
- Carlsaw, K. S., Lee, L. A., Reddington, C. L., Pringle, K. J., Rap, A., Forster, P. M., Mann, G. W., Spracklen, D. V., Woodhouse, M. T., Regayre, L. A., and Pierce, J. R.: Large contribution of natural aerosols to uncertainty in indirect forcing, *Nature*, 503, 67–71, <https://doi.org/10.1038/nature12674>, 2013.
- Collins, D. B., Bertram, T. H., Sultana, C. M., Lee, C., Axson, J. L., and Prather, K. A.: Phytoplankton blooms weakly influence the cloud forming ability of sea spray aerosol, *Geophys. Res. Lett.*, 43, 9975–9983, <https://doi.org/10.1002/2016GL069922>, 2016.
- Danilov, S., Sidorenko, D., Wang, Q., and Jung, T.: The Finite-volume Sea ice–Ocean Model (FESOM2), *Geosci. Model Dev.*, 10, 765–789, <https://doi.org/10.5194/gmd-10-765-2017>, 2017.
- DeMott, P. J., Hill, T. C., McCluskey, C. S., Prather, K. A., Collins, D. B., Sullivan, R. C., Ruppel, M. J., Mason, R. H., Irish, V. E., Lee, T., Hwang, C. Y., Rhee, T. S., Snider, J. R., McMeeking, G. R., Dhaniyala, S., Lewis, E. R., Wentzell, J. J., Abbatt, J., Lee, C., Sultana, C. M., Ault, A. P., Axson, J. L., Martinez, M. D., Venero, I., Santos-Figueroa, G., Stokes, M. D., Deane, G. B., Mayol-Bracero, O. L., Grassian, V. H., Bertram, T. H., Bertram, A. K., Moffett, B. F., and Franc, G. D.: Sea spray aerosol as a unique source of ice nucleating particles, *P. Natl. Acad. Sci. USA*, 113, 5797–5803, <https://doi.org/10.1073/pnas.1514034112>, 2016.
- Engel, A. and Galgani, L.: The organic sea-surface microlayer in the upwelling region off the coast of Peru and potential implications for air–sea exchange processes, *Biogeosciences*, 13, 989–1007, <https://doi.org/10.5194/bg-13-989-2016>, 2016.
- Engel, A., Goldthwait, S., Passow, U., and Alldredge, A.: Temporal decoupling of carbon and nitrogen dynamics in a mesocosm diatom bloom, *Limnol. Oceanogr.*, 47, 753–761, <https://doi.org/10.4319/lo.2002.47.3.0753>, 2002.
- Engel, A., Thoms, S., Riebesell, U., Rochelle-Newall, E., and Zondervan, I.: Polysaccharide aggregation as a potential sink of marine dissolved organic carbon, *Nature*, 428, 929–932, <https://doi.org/10.1038/nature02453>, 2004.
- Engel, A., Bange, H. W., Cunliffe, M., Burrows, S. M., Friedrichs, G., Galgani, L., Herrmann, H., Hertkorn, N., Johnson, M., Liss, P. S., Quinn, P. K., Schartau, M., Soloviev, A., Stolle, C., Upstill-Goddard, R. C., van Pinxteren, M., and Zäncker, B.: The Ocean's Vital Skin: Toward an Integrated Understanding of the Sea Surface Microlayer, *Frontiers in Marine Science*, 4, 165, <https://doi.org/10.3389/fmars.2017.00165>, 2017.
- Engel, A., Endres, S., Galgani, L., and Schartau, M.: Marvelous Marine Microgels: On the Distribution and Impact of Gel-Like Particles in the Oceanic Water-Column, *Frontiers in Marine Science*, 7, 405, <https://doi.org/10.3389/fmars.2020.00405>, 2020.
- Facchini, M. C., Rinaldi, M., Decesari, S., Carbone, C., Finessi, E., Mircea, M., Fuzzi, S., Ceburnis, D., Flanagan, R., Nilsson, E. D., de Leeuw, G., Martino, M., Woeltjen, J., and O'Dowd, C. D.: Primary submicron marine aerosol dominated by insoluble organic colloids and aggregates, *Geophys. Res. Lett.*, 35, L17814, <https://doi.org/10.1029/2008GL034210>, 2008.
- Feltracco, M., Barbaro, E., Kirchgeorg, T., Spolaor, A., Turetta, C., Zangrando, R., Barbante, C., and Gambaro, A.: Free and combined L- and D-amino acids in Arctic aerosol, *Chemosphere*, 220, 412–421, <https://doi.org/10.1016/j.chemosphere.2018.12.147>, 2019.
- Frka, S., Gašparović, B., Marić, D., Godrijan, J., Djakovac, T., Vojvodić, V., Dautović, J., and Kozarac, Z.: Phytoplankton driven distribution of dissolved and particulate lipids in a semi-enclosed temperate sea (Mediterranean): Spring to summer situation, *Estuar. Coast. Shelf S.*, 93, 290–304, <https://doi.org/10.1016/j.ecss.2011.04.017>, 2011.
- Frka, S., Pogorzelski, S., Kozarac, Z., and Čosović, B.: Physicochemical Signatures of Natural Sea Films from Mid-

- dle Adriatic Stations, *J. Phys. Chem. A*, 116, 6552–6559, <https://doi.org/10.1021/jp212430a>, 2012.
- Frossard, A. A., Russell, L. M., Burrows, S. M., Elliott, S. M., Bates, T. S., and Quinn, P. K.: Sources and composition of submicron organic mass in marine aerosol particles, *J. Geophys. Res.-Atmos.*, 119, 12977–13003, <https://doi.org/10.1002/2014JD021913>, 2014.
- Galí, M., Levasseur, M., Devred, E., Simó, R., and Babin, M.: Sea-surface dimethylsulfide (DMS) concentration from satellite data at global and regional scales, *Biogeosciences*, 15, 3497–3519, <https://doi.org/10.5194/bg-15-3497-2018>, 2018.
- Gantt, B. and Meskhidze, N.: The physical and chemical characteristics of marine primary organic aerosol: a review, *Atmos. Chem. Phys.*, 13, 3979–3996, <https://doi.org/10.5194/acp-13-3979-2013>, 2013.
- Gantt, B., Meskhidze, N., Facchini, M. C., Rinaldi, M., Ceburnis, D., and O’Dowd, C. D.: Wind speed dependent size-resolved parameterization for the organic mass fraction of sea spray aerosol, *Atmos. Chem. Phys.*, 11, 8777–8790, <https://doi.org/10.5194/acp-11-8777-2011>, 2011.
- Gantt, B., Johnson, M. S., Meskhidze, N., Sciare, J., Ovadnevaite, J., Ceburnis, D., and O’Dowd, C. D.: Model evaluation of marine primary organic aerosol emission schemes, *Atmos. Chem. Phys.*, 12, 8553–8566, <https://doi.org/10.5194/acp-12-8553-2012>, 2012a.
- Gantt, B., Xu, J., Meskhidze, N., Zhang, Y., Nenes, A., Ghan, S. J., Liu, X., Easter, R., and Zaveri, R.: Global distribution and climate forcing of marine organic aerosol – Part 2: Effects on cloud properties and radiative forcing, *Atmos. Chem. Phys.*, 12, 6555–6563, <https://doi.org/10.5194/acp-12-6555-2012>, 2012b.
- Gantt, B., Johnson, M. S., Crippa, M., Prévôt, A. S. H., and Meskhidze, N.: Implementing marine organic aerosols into the GEOS-Chem model, *Geosci. Model Dev.*, 8, 619–629, <https://doi.org/10.5194/gmd-8-619-2015>, 2015.
- Gao, C. Y., Heald, C. L., Katich, J. M., Luo, G., and Yu, F.: Remote Aerosol Simulated During the Atmospheric Tomography (ATom) Campaign and Implications for Aerosol Lifetime, *J. Geophys. Res.-Atmos.*, 127, e2022JD036524, <https://doi.org/10.1029/2022JD036524>, 2022.
- Garcia, H., Weathers, K., Paver, C., Smolyar, I., Boyer, T., Locarnini, M., Zweng, M., Mishonov, A., Baranova, O., Seidov, D., and Reagan, J.: World Ocean Atlas 2018, Volume 3: Dissolved Oxygen, Apparent Oxygen Utilization, and Dissolved Oxygen Saturation., Tech. rep., 965 <https://archimer.ifremer.fr/doc/00651/76337/> (last access: 1 July 2025), 2019a.
- Garcia, H., Weathers, K., Paver, C., Smolyar, I., Boyer, T., Locarnini, M., Zweng, M., Mishonov, A., Baranova, O., Seidov, D., and Reagan, J.: World Ocean Atlas 2018. Vol. 4: Dissolved Inorganic Nutrients (phosphate, nitrate and nitrate+nitrite, silicate), Tech. rep., <https://archimer.ifremer.fr/doc/00651/76336/> (last access: 1 July 2025), 2019b.
- Geider, R. J., MacIntyre, H. L., and Kana, T. M.: A dynamic regulatory model of phytoplankton acclimation to light, nutrients, and temperature, *Limnol. Oceanogr.*, 43, 679–694, <https://doi.org/10.4319/lo.1998.43.4.0679>, 1998.
- Gong, S. L.: A parameterization of sea-salt aerosol source function for sub- and super-micron particles, *Global Biogeochem. Cy.*, 17, 1097, <https://doi.org/10.1029/2003GB002079>, 2003.
- Granum, E., Kirkvold, S., and Mykkestad, S.: Cellular and extracellular production of carbohydrates and amino acids by the marine diatom *Skeletonema costatum*: diel variations and effects of N depletion, *Mar. Ecol. Prog. Ser.*, 242, 83–94, <https://doi.org/10.3354/meps242083>, 2002.
- Grythe, H., Ström, J., Krejci, R., Quinn, P., and Stohl, A.: A review of sea-spray aerosol source functions using a large global set of sea salt aerosol concentration measurements, *Atmos. Chem. Phys.*, 14, 1277–1297, <https://doi.org/10.5194/acp-14-1277-2014>, 2014.
- Guelle, W., Schulz, M., Balkanski, Y., and Dentener, F.: Influence of the source formulation on modeling the atmospheric global distribution of sea salt aerosol, *J. Geophys. Res.-Atmos.*, 106, 27509–27524, <https://doi.org/10.1029/2001JD900249>, 2001.
- Gürses, Ö., Oziel, L., Karakuş, O., Sidorenko, D., Völker, C., Ye, Y., Zeising, M., Butzin, M., and Hauck, J.: Ocean biogeochemistry in the coupled ocean–sea ice–biogeochemistry model FESOM2.1–REcoM3, *Geosci. Model Dev.*, 16, 4883–4936, <https://doi.org/10.5194/gmd-16-4883-2023>, 2023.
- Guschina, I. A. and Harwood, J. L.: Algal lipids and effect of the environment on their biochemistry, Springer New York, 1–24, [https://doi.org/10.1007/978-0-387-89366-2\\_1](https://doi.org/10.1007/978-0-387-89366-2_1), 2009.
- Hama, T. and Yanagi, K.: Production and neutral aldose composition of dissolved carbohydrates excreted by natural marine phytoplankton populations, *Limnol. Oceanogr.*, 46, 1945–1955, <https://doi.org/10.4319/lo.2001.46.8.1945>, 2001.
- HAMMOZ: ECHAM-HAMMOZ, [https://redmine.hammoz.ethz.ch/projects/hammoz/wiki/I\\_Licencing\\_conditions](https://redmine.hammoz.ethz.ch/projects/hammoz/wiki/I_Licencing_conditions), last access: 22 November 2024.
- Han, Z., Li, J., Yao, X., and Tan, S.: A regional model study of the characteristics and indirect effects of marine primary organic aerosol in springtime over East Asia, *Atmos. Environ.*, 197, 22–35, <https://doi.org/10.1016/j.atmosenv.2018.10.014>, 2019.
- Hansell, D. A., Carlson, C. A., and Schlitzer, R.: Net removal of major marine dissolved organic carbon fractions in the subsurface ocean, *Global Biogeochem. Cy.*, 26, GB1016, <https://doi.org/10.1029/2011GB004069>, 2012.
- Harwood, J. L. and Guschina, I. A.: The versatility of algae and their lipid metabolism, *Biochimie*, 91, 679–684, <https://doi.org/10.1016/j.biochi.2008.11.004>, 2009.
- Hasencz, E. S., Kaluarachchi, C. P., Lee, H. D., Tivanski, A. V., and Stone, E. A.: Saccharide Transfer to Sea Spray Aerosol Enhanced by Surface Activity, Calcium, and Protein Interactions, *ACS Earth and Space Chemistry*, 3, 2539–2548, <https://doi.org/10.1021/acsearthspacechem.9b00197>, 2019.
- Hawkins, L. N. and Russell, L. M.: Polysaccharides, Proteins, and Phytoplankton Fragments: Four Chemically Distinct Types of Marine Primary Organic Aerosol Classified by Single Particle Spectromicroscopy, *Adv. Meteorol.*, 2010, 1–14, <https://doi.org/10.1155/2010/612132>, 2010.
- Hellebust, J. A.: EXCRETION OF SOME ORGANIC COMPOUNDS BY MARINE PHYTOPLANKTON, *Limnol. Oceanogr.*, 10, 192–206, <https://doi.org/10.4319/lo.1965.10.2.0192>, 1965.
- Hodzic, A., Campuzano-Jost, P., Bian, H., Chin, M., Colarco, P. R., Day, D. A., Froyd, K. D., Heinold, B., Jo, D. S., Katich, J. M., Kodros, J. K., Nault, B. A., Pierce, J. R., Ray, E., Schacht, J., Schill, G. P., Schroder, J. C., Schwarz, J. P., Sueper, D. T., Tegen, I., Tilmes, S., Tsigaridis, K., Yu, P., and Jimenez,

- J. L.: Characterization of organic aerosol across the global remote troposphere: a comparison of ATom measurements and global chemistry models, *Atmos. Chem. Phys.*, 20, 4607–4635, <https://doi.org/10.5194/acp-20-4607-2020>, 2020.
- Hopkinson, C. S., Vallino, J. J., and Nolin, A.: Decomposition of dissolved organic matter from the continental margin, *Deep-Sea Res. Pt. II*, 49, 4461–4478, [https://doi.org/10.1016/S0967-0645\(02\)00125-X](https://doi.org/10.1016/S0967-0645(02)00125-X), 2002.
- Huang, W. T. K., Ickes, L., Tegen, I., Rinaldi, M., Ceburnis, D., and Lohmann, U.: Global relevance of marine organic aerosol as ice nucleating particles, *Atmos. Chem. Phys.*, 18, 11423–11445, <https://doi.org/10.5194/acp-18-11423-2018>, 2018.
- Karl, D. M. and Björkman, K. M.: Dynamics of Dissolved Organic Phosphorus, Elsevier, 233–334, <https://doi.org/10.1016/B978-0-12-405940-5.00005-4>, 2015.
- Keene, W. C., Maring, H., Maben, J. R., Kieber, D. J., Pszenny, A. A. P., Dahl, E. E., Izaguirre, M. A., Davis, A. J., Long, M. S., Zhou, X., Smoydzin, L., and Sander, R.: Chemical and physical characteristics of nascent aerosols produced by bursting bubbles at a model air-sea interface, *J. Geophys. Res.-Atmos.*, 112, D21202, <https://doi.org/10.1029/2007JD008464>, 2007.
- Koldunov, N. V., Aizinger, V., Rakowsky, N., Scholz, P., Sidorenko, D., Danilov, S., and Jung, T.: Scalability and some optimization of the Finite-volume Sea ice–Ocean Model, Version 2.0 (FESOM2), *Geosci. Model Dev.*, 12, 3991–4012, <https://doi.org/10.5194/gmd-12-3991-2019>, 2019.
- Kuznetsova, M. and Lee, C.: Dissolved free and combined amino acids in nearshore seawater, sea surface microlayers and foams: Influence of extracellular hydrolysis, *Aquat. Sci.*, 64, 252–268, <https://doi.org/10.1007/s00027-002-8070-0>, 2002.
- Kuznetsova, M., Lee, C., Aller, J., and Frew, N.: Enrichment of amino acids in the sea surface microlayer at coastal and open ocean sites in the North Atlantic Ocean, *Limnol. Oceanogr.*, 49, 1605–1619, <https://doi.org/10.4319/lo.2004.49.5.1605>, 2004.
- Lancelot, C.: Extracellular release of small and large molecules by phytoplankton in the Southern Bight of the North Sea, *Estuar. Coast. Shelf S.*, 18, 65–77, [https://doi.org/10.1016/0272-7714\(84\)90007-6](https://doi.org/10.1016/0272-7714(84)90007-6), 1984.
- Lapere, R., Thomas, J. L., Marelle, L., Ekman, A. M. L., Frey, M. M., Lund, M. T., Makkonen, R., Ranjithkumar, A., Salter, M. E., Samset, B. H., Schulz, M., Sogacheva, L., Yang, X., and Zieger, P.: The Representation of Sea Salt Aerosols and Their Role in Polar Climate Within CMIP6, *J. Geophys. Res.-Atmos.*, 128, e2022JD038235, <https://doi.org/10.1029/2022JD038235>, 2023.
- Lauvset, S. K., Key, R. M., Olsen, A., van Heuven, S., Velo, A., Lin, X., Schirnick, C., Kozyr, A., Tanhua, T., Hoppema, M., Jutterström, S., Steinfeldt, R., Jeansson, E., Ishii, M., Perez, F. F., Suzuki, T., and Watelet, S.: A new global interior ocean mapped climatology: the  $1^\circ \times 1^\circ$  GLODAP version 2, *Earth Syst. Sci. Data*, 8, 325–340, <https://doi.org/10.5194/essd-8-325-2016>, 2016.
- Leck, C., Gao, Q., Mashayekhy Rad, F., and Nilsson, U.: Size-resolved atmospheric particulate polysaccharides in the high summer Arctic, *Atmos. Chem. Phys.*, 13, 12573–12588, <https://doi.org/10.5194/acp-13-12573-2013>, 2013.
- Leon-Marcos, A. and Heinold, B.: Simulation experiment configuration files for the manuscript “Modelling emission and transport of key components of primary marine organic aerosol using the global aerosol-climate model ECHAM6.3–HAM2.3”, Zenodo [code], <https://doi.org/10.5281/zenodo.14203456>, 2024a.
- Leon-Marcos, A. and Heinold, B.: Aerosol model code for the paper publication “Modelling emission and transport of key components of primary marine organic aerosol using the global aerosol-climate model ECHAM6.3–HAM2.3”, Zenodo [code], <https://doi.org/10.5281/zenodo.14193491>, 2024b.
- Leon-Marcos, A., Zeising, M., van Pinxteren, M., Zeppenfeld, S., Bracher, A., Barbaro, E., Engel, A., Feltracco, M., Tegen, I., and Heinold, B.: Data for paper publication “Modelling emission and transport of key components of primary marine organic aerosol using the global aerosol-climate model ECHAM6.3–HAM2.3” (v2.0), Zenodo [data set], <https://doi.org/10.5281/zenodo.15172565>, 2025.
- Lewis, R. and Schwartz, E.: Sea Salt Aerosol Production: Mechanisms, Methods, Measurements and Models – A Critical Review, vol. 152, American Geophysical Union, ISBN 0-87590-417-3, <https://doi.org/10.1029/GM152>, 2004.
- Lin, S.-J. and Rood, R. B.: Multidimensional Flux-Form Semi-Lagrangian Transport Schemes, *Mon. Weather Rev.*, 124, 2046–2070, [https://doi.org/10.1175/1520-0493\(1996\)124<2046:MFFSLT>2.0.CO;2](https://doi.org/10.1175/1520-0493(1996)124<2046:MFFSLT>2.0.CO;2), 1996.
- Link, K. A., Spurzem, G. N., Tuladhar, A., Chase, Z., Wang, Z., Wang, H., and Walker, R. A.: Organic Enrichment at Aqueous Interfaces: Cooperative Adsorption of Glucuronic Acid to DPPC Monolayers Studied with Vibrational Sum Frequency Generation, *J. Phys. Chem. A*, 123, 5621–5632, <https://doi.org/10.1021/acs.jpca.9b02255>, 2019.
- Lohmann, U. and Hoose, C.: Sensitivity studies of different aerosol indirect effects in mixed-phase clouds, *Atmos. Chem. Phys.*, 9, 8917–8934, <https://doi.org/10.5194/acp-9-8917-2009>, 2009.
- Lohmann, U. and Neubauer, D.: The importance of mixed-phase and ice clouds for climate sensitivity in the global aerosol-climate model ECHAM6-HAM2, *Atmos. Chem. Phys.*, 18, 8807–8828, <https://doi.org/10.5194/acp-18-8807-2018>, 2018.
- Lohmann, U., Stier, P., Hoose, C., Ferrachat, S., Kloster, S., Roeckner, E., and Zhang, J.: Cloud microphysics and aerosol indirect effects in the global climate model ECHAM5-HAM, *Atmos. Chem. Phys.*, 7, 3425–3446, <https://doi.org/10.5194/acp-7-3425-2007>, 2007.
- Long, M. S., Keene, W. C., Kieber, D. J., Erickson, D. J., and Maring, H.: A sea-state based source function for size- and composition-resolved marine aerosol production, *Atmos. Chem. Phys.*, 11, 1203–1216, <https://doi.org/10.5194/acp-11-1203-2011>, 2011.
- Mague, T. H., Friberg, E., Hughes, D. J., and Morris, I.: Extracellular release of carbon by marine phytoplankton; a physiological approach1, *Limnol. Oceanogr.*, 25, 262–279, <https://doi.org/10.4319/lo.1980.25.2.0262>, 1980.
- Maßmig, M. and Engel, A.: Dissolved Organic Matter in the Upwelling System off Peru: Imprints of Bacterial Activity and Water Mass Characteristics, *J. Geophys. Res.-Biogeo.*, 126, e2020JG006048, <https://doi.org/10.1029/2020JG006048>, 2021.
- McCluskey, C. S., Hill, T. C. J., Sultana, C. M., Laskina, O., Trueblood, J., Santander, M. V., Beall, C. M., Michaud, J. M., Kreidenweis, S. M., Prather, K. A., Grassian, V., and DeMott, P. J.: A Mesocosm Double Feature: Insights into the Chemical Make-up of Marine Ice Nucleating Particles, *J. Atmos. Sci.*, 75, 2405–2423, <https://doi.org/10.1175/JAS-D-17-0155.1>, 2018a.

- McCluskey, C. S., Ovadnevaite, J., Rinaldi, M., Atkinson, J., Berosi, F., Ceburnis, D., Marullo, S., Hill, T. C. J., Lohmann, U., Kanji, Z. A., O'Dowd, C., Kreidenweis, S. M., and DeMott, P. J.: Marine and Terrestrial Organic Ice-Nucleating Particles in Pristine Marine to Continentally Influenced Northeast Atlantic Air Masses, *J. Geophys. Res.-Atmos.*, 123, 6196–6212, <https://doi.org/10.1029/2017JD028033>, 2018b.
- Meskhidze, N., Xu, J., Gantt, B., Zhang, Y., Nenes, A., Ghan, S. J., Liu, X., Easter, R., and Zaveri, R.: Global distribution and climate forcing of marine organic aerosol: 1. Model improvements and evaluation, *Atmos. Chem. Phys.*, 11, 11689–11705, <https://doi.org/10.5194/acp-11-11689-2011>, 2011.
- Murphy, D. M., Anderson, J. R., Quinn, P. K., McInnes, L. M., Brechtel, F. J., Kreidenweis, S. M., Middlebrook, A. M., Pósfai, M., Thomson, D. S., and Buseck, P. R.: Influence of sea-salt on aerosol radiative properties in the Southern Ocean marine boundary layer, *Nature*, 392, 62–65, <https://doi.org/10.1038/32138>, 1998.
- Mykkestad, S., Haug, A., and Larsen, B.: Production of carbohydrates by the marine diatom *Chaetoceros affinis* var. *willei* (Gran) Hustedt. II. Preliminary investigation of the extracellular polysaccharide, *J. Exp. Mar. Biol. Ecol.*, 9, 137–144, [https://doi.org/10.1016/0022-0981\(72\)90042-1](https://doi.org/10.1016/0022-0981(72)90042-1), 1972.
- Mykkestad, S., Holm-Hansen, O., Vårum, K. M., and Volcani, B. E.: Rate of release of extracellular amino acids and carbohydrates from the marine diatom *Chaetoceros affinis*, *J. Plankton Res.*, 11, 763–773, <https://doi.org/10.1093/plankt/11.4.763>, 1989.
- Mykkestad, S. M.: Release of extracellular products by phytoplankton with special emphasis on polysaccharides, *Sci. Total Environ.*, 165, 155–164, [https://doi.org/10.1016/0048-9697\(95\)04549-G](https://doi.org/10.1016/0048-9697(95)04549-G), 1995.
- Mykkestad, S. M.: Dissolved Organic Carbon from Phytoplankton, Springer Berlin Heidelberg, 111–148, ISBN 978-3-540-48776-0, [https://doi.org/10.1007/10683826\\_5](https://doi.org/10.1007/10683826_5), 2000.
- Mårtensson, E. M., Nilsson, E. D., de Leeuw, G., Cohen, L. H., and Hansson, H.: Laboratory simulations and parameterization of the primary marine aerosol production, *J. Geophys. Res.-Atmos.*, 108, 4297, <https://doi.org/10.1029/2002JD002263>, 2003.
- Obernosterer, I. and Herndl, G.: Phytoplankton extracellular release and bacterial growth: dependence on the inorganic N: P ratio, *Mar. Ecol. Prog. Ser.*, 116, 247–257, <https://doi.org/10.3354/meps116247>, 1995.
- O'Dowd, C. D., Smith, M. H., Consterdine, I. E., and Lowe, J. A.: Marine aerosol, sea-salt, and the marine sulphur cycle: a short review, *Atmos. Environ.*, 31, 73–80, [https://doi.org/10.1016/S1352-2310\(96\)00106-9](https://doi.org/10.1016/S1352-2310(96)00106-9), 1997.
- O'Dowd, C. D., Langmann, B., Varghese, S., Scannell, C., Ceburnis, D., and Facchini, M. C.: A combined organic-inorganic sea-spray source function, *Geophys. Res. Lett.*, 35, L01801, <https://doi.org/10.1029/2007GL030331>, 2008.
- Ogunro, O. O., Burrows, S. M., Elliott, S., Frossard, A. A., Hoffman, F., Letscher, R. T., Moore, J. K., Russell, L. M., Wang, S., and Wingerter, O. W.: Global distribution and surface activity of macromolecules in offline simulations of marine organic chemistry, *Biogeochemistry*, 126, 25–56, <https://doi.org/10.1007/s10533-015-0136-x>, 2015.
- Pai, S. J., Heald, C. L., Pierce, J. R., Farina, S. C., Marais, E. A., Jimenez, J. L., Campuzano-Jost, P., Nault, B. A., Middlebrook, A. M., Coe, H., Shilling, J. E., Bahreini, R., Dingle, J. H., and Vu, K.: An evaluation of global organic aerosol schemes using airborne observations, *Atmos. Chem. Phys.*, 20, 2637–2665, <https://doi.org/10.5194/acp-20-2637-2020>, 2020.
- Pandis, S. N., Russell, L. M., and Seinfeld, J. H.: The relationship between DMS flux and CCN concentration in remote marine regions, *J. Geophys. Res.-Atmos.*, 99, 16945–16957, <https://doi.org/10.1029/94JD01119>, 1994.
- Parrish, C. C. and Wangersky, P. J.: Particulate and dissolved lipid classes in cultures of *Phaeodactylum tricornutum* grown in cage culture turbidostats with a range of nitrogen supply rates, *Mar. Ecol. Prog. Ser.*, 35, 119–128, <http://www.jstor.org/stable/24825016> (last access: 1 July 2025), 1987.
- Parrish, C. C., Bodennec, G., Sebedio, J.-L., and Gentien, P.: Intra- and extracellular lipids in cultures of the toxic dinoflagellate, *Gyrodinium aureolum*, *Phytochemistry*, 32, 291–295, [https://doi.org/10.1016/S0031-9422\(00\)94983-5](https://doi.org/10.1016/S0031-9422(00)94983-5), 1993.
- Parrish, C. C., Bodennec, G., and Gentien, P.: Time courses of intracellular and extracellular lipid classes in batch cultures of the toxic dinoflagellate, *Gymnodinium cf. nagasakiense*, *Mar. Chem.*, 48, 71–82, [https://doi.org/10.1016/0304-4203\(94\)90063-9](https://doi.org/10.1016/0304-4203(94)90063-9), 1994.
- Pincus, R. and Stevens, B.: Paths to accuracy for radiation parameterizations in atmospheric models, *J. Adv. Model. Earth Sy.*, 5, 225–233, <https://doi.org/10.1002/jame.20027>, 2013.
- Pinxteren, M. V., Barthel, S., Fomba, K. W., Müller, K., Tümppling, W. V., and Herrmann, H.: The influence of environmental drivers on the enrichment of organic carbon in the sea surface microlayer and in submicron aerosol particles – measurements from the Atlantic Ocean, *Elementa*, 5, 35, <https://doi.org/10.1525/elementa.225>, 2017.
- Prather, K. A., Bertram, T. H., Grassian, V. H., Deane, G. B., Stokes, M. D., DeMott, P. J., Aluwihare, L. I., Palenik, B. P., Azam, F., Seinfeld, J. H., Moffet, R. C., Molina, M. J., Cappa, C. D., Geiger, F. M., Roberts, G. C., Russell, L. M., Ault, A. P., Baltrusaitis, J., Collins, D. B., Corrigan, C. E., Cuadrado-Rodriguez, L. A., Ebben, C. J., Forestieri, S. D., Guasco, T. L., Hersey, S. P., Kim, M. J., Lambert, W. F., Modini, R. L., Mui, W., Pedler, B. E., Ruppel, M. J., Ryder, O. S., Schoepp, N. G., Sullivan, R. C., and Zhao, D.: Bringing the ocean into the laboratory to probe the chemical complexity of sea spray aerosol, *P. Natl. Acad. Sci. USA*, 110, 7550–7555, <https://doi.org/10.1073/pnas.1300262110>, 2013.
- Rastelli, E., Corinaldesi, C., Dell'Anno, A., Martire, M. L., Greco, S., Facchini, M. C., Rinaldi, M., O'Dowd, C., Ceburnis, D., and Danovaro, R.: Transfer of labile organic matter and microbes from the ocean surface to the marine aerosol: an experimental approach, *Sci. Rep.*, 7, 11475, <https://doi.org/10.1038/s41598-017-10563-z>, 2017.
- Regayre, L. A., Schmale, J., Johnson, J. S., Tatzelt, C., Baccharini, A., Henning, S., Yoshioka, M., Stratmann, F., Gysel-Beer, M., Grosvenor, D. P., and Carslaw, K. S.: The value of remote marine aerosol measurements for constraining radiative forcing uncertainty, *Atmos. Chem. Phys.*, 20, 10063–10072, <https://doi.org/10.5194/acp-20-10063-2020>, 2020.
- Reinthal, T., Sintes, E., and Herndl, G. J.: Dissolved organic matter and bacterial production and respiration in the sea-surface microlayer of the open Atlantic and the western Mediterranean Sea, *Limnol. Oceanogr.*, 53, 122–136, <https://doi.org/10.4319/lo.2008.53.1.0122>, 2008.

- Repeta, D. J.: Chapter 2 – Chemical Characterization and Cycling of Dissolved Organic Matter, Academic Press, second edition, 21–63, ISBN 978-0-12-405940-5, <https://doi.org/10.1016/B978-0-12-405940-5.00002-9>, 2015.
- Rinaldi, M., Fuzzi, S., Decesari, S., Marullo, S., Santoleri, R., Provenzale, A., von Hardenberg, J., Ceburnis, D., Vaishya, A., O’Dowd, C. D., and Facchini, M. C.: Is chlorophyll-*a* the best surrogate for organic matter enrichment in submicron primary marine aerosol?, *J. Geophys. Res.-Atmos.*, 118, 4964–4973, <https://doi.org/10.1002/jgrd.50417>, 2013.
- Rinaldi, M., Paglione, M., Decesari, S., Harrison, R. M., Beddows, D. C., Ovadnevaite, J., Ceburnis, D., O’Dowd, C. D., Simó, R., and Osto, M. D.: Contribution of Water-Soluble Organic Matter from Multiple Marine Geographic Eco-Regions to Aerosols around Antarctica, *Environ. Sci. Technol.*, 54, 7807–7817, <https://doi.org/10.1021/acs.est.0c00695>, 2020.
- Russell, L. M., Hawkins, L. N., Frossard, A. A., Quinn, P. K., and Bates, T. S.: Carbohydrate-like composition of submicron atmospheric particles and their production from ocean bubble bursting, *P. Natl. Acad. Sci. USA*, 107, 6652–6657, <https://doi.org/10.1073/pnas.0908905107>, 2010.
- Schartau, M., Engel, A., Schröter, J., Thoms, S., Völker, C., and Wolf-Gladrow, D.: Modelling carbon overconsumption and the formation of extracellular particulate organic carbon, *Biogeochemistry*, 4, 433–454, <https://doi.org/10.5194/bg-4-433-2007>, 2007.
- Schmitt-Kopplin, P., Liger-Belair, G., Koch, B. P., Flerus, R., Kattner, G., Harir, M., Kanawati, B., Lucio, M., Tziotis, D., Hertkorn, N., and Gebefügi, I.: Dissolved organic matter in sea spray: a transfer study from marine surface water to aerosols, *Biogeochemistry*, 9, 1571–1582, <https://doi.org/10.5194/bg-9-1571-2012>, 2012.
- Schourup-Kristensen, V., Sidorenko, D., Wolf-Gladrow, D. A., and Völker, C.: A skill assessment of the biogeochemical model REcoM2 coupled to the Finite Element Sea Ice–Ocean Model (FESOM 1.3), *Geosci. Model Dev.*, 7, 2769–2802, <https://doi.org/10.5194/gmd-7-2769-2014>, 2014.
- Schourup-Kristensen, V., Wekerle, C., Wolf-Gladrow, D. A., and Völker, C.: Arctic Ocean biogeochemistry in the high resolution FESOM 1.4-REcoM2 model, *Prog. Oceanogr.*, 168, 65–81, <https://doi.org/10.1016/j.pocean.2018.09.006>, 2018.
- Sciare, J., Oikonomou, K., Cachier, H., Mihalopoulos, N., Andreae, M. O., Maenhaut, W., and Sarda-Estève, R.: Aerosol mass closure and reconstruction of the light scattering coefficient over the Eastern Mediterranean Sea during the MINOS campaign, *Atmos. Chem. Phys.*, 5, 2253–2265, <https://doi.org/10.5194/acp-5-2253-2005>, 2005.
- Seinfeld, J. H. and Pandis, S. N.: Atmospheric chemistry and physics: From air pollution to climate change, John Wiley & Sons, ISBN 9780471720188, 2006.
- Sellegri, K., O’Dowd, C. D., Yoon, Y. J., Jennings, S. G., and de Leeuw, G.: Surfactants and submicron sea spray generation, *J. Geophys. Res.-Atmos.*, 111, D22215, <https://doi.org/10.1029/2005JD006658>, 2006.
- Simó, R.: From cells to globe: approaching the dynamics of DMS(P) in the ocean at multiple scales, *Can. J. Fish. Aquat. Sci.*, 61, 673–684, <https://doi.org/10.1139/f04-030>, 2004.
- Sofiev, M., Soares, J., Prank, M., de Leeuw, G., and Kukkonen, J.: A regional-to-global model of emission and transport of sea salt particles in the atmosphere, *J. Geophys. Res.-Atmos.*, 116, D21302, <https://doi.org/10.1029/2010JD014713>, 2011.
- Steele, M., Morley, R., and Ermold, W.: PHC: A Global Ocean Hydrography with a High-Quality Arctic Ocean, *J. Climate*, 14, 2079–2087, [https://doi.org/10.1175/1520-0442\(2001\)014<2079:PAGOHW>2.0.CO;2](https://doi.org/10.1175/1520-0442(2001)014<2079:PAGOHW>2.0.CO;2), 2001.
- Stefan, R. L. and Szeri, A. J.: Surfactant Scavenging and Surface Deposition by Rising Bubbles, *J. Colloid Interf. Sci.*, 212, 1–13, <https://doi.org/10.1006/jcis.1998.6037>, 1999.
- Stevens, B., Giorgetta, M., Esch, M., Mauritsen, T., Crueger, T., Rast, S., Salzmann, M., Schmidt, H., Bader, J., Block, K., Brokopf, R., Fast, I., Kinne, S., Kornbluh, L., Lohmann, U., Pincus, R., Reichler, T., and Roeckner, E.: Atmospheric component of the MPI-M Earth System Model: ECHAM6, *J. Adv. Model. Earth Sy.*, 5, 146–172, <https://doi.org/10.1002/jame.20015>, 2013.
- Stier, P., Feichter, J., Kinne, S., Kloster, S., Vignati, E., Wilson, J., Ganzeveld, L., Tegen, I., Werner, M., Balkanski, Y., Schulz, M., Boucher, O., Minikin, A., and Petzold, A.: The aerosol-climate model ECHAM5-HAM, *Atmos. Chem. Phys.*, 5, 1125–1156, <https://doi.org/10.5194/acp-5-1125-2005>, 2005.
- Taylor, K. E., Williamson, D. L., and Zwiers, F. W.: The Sea Surface Temperature and Sea-Ice Concentration Boundary Conditions for AMIP II Simulations, Program for Climate Model Diagnosis and Intercomparison (PCMDI) Report 60, Lawrence Livermore National Laboratory, Livermore, California, <https://pcmdi.llnl.gov/report/ab60.html> (last access: 1 July 2025), 2000.
- Tegen, I., Neubauer, D., Ferrachat, S., Siegenthaler-Le Drian, C., Bey, I., Schutgens, N., Stier, P., Watson-Parris, D., Stanelle, T., Schmidt, H., Rast, S., Kokkola, H., Schultz, M., Schroeder, S., Daskalakis, N., Barthel, S., Heinold, B., and Lohmann, U.: The global aerosol–climate model ECHAM6.3–HAM2.3 – Part 1: Aerosol evaluation, *Geosci. Model Dev.*, 12, 1643–1677, <https://doi.org/10.5194/gmd-12-1643-2019>, 2019.
- Thornton, D. C.: Dissolved organic matter (DOM) release by phytoplankton in the contemporary and future ocean, *Eur. J. Phycol.*, 49, 20–46, <https://doi.org/10.1080/09670262.2013.875596>, 2014.
- Triesch, N., van Pinxteren, M., Engel, A., and Herrmann, H.: Concerted measurements of free amino acids at the Cabo Verde islands: high enrichments in submicron sea spray aerosol particles and cloud droplets, *Atmos. Chem. Phys.*, 21, 163–181, <https://doi.org/10.5194/acp-21-163-2021>, 2021a.
- Triesch, N., van Pinxteren, M., Frka, S., Stolle, C., Spranger, T., Hoffmann, E. H., Gong, X., Wex, H., Schulz-Bull, D., Gašparović, B., and Herrmann, H.: Concerted measurements of lipids in seawater and on submicrometer aerosol particles at the Cabo Verde islands: biogenic sources, selective transfer and high enrichments, *Atmos. Chem. Phys.*, 21, 4267–4283, <https://doi.org/10.5194/acp-21-4267-2021>, 2021b.
- Tsujino, H., Urakawa, S., Nakano, H., Small, R. J., Kim, W. M., Yeager, S. G., Danabasoglu, G., Suzuki, T., Bamber, J. L., Bentsen, M., Böning, C. W., Bozec, A., Chassignet, E. P., Curchitsier, E., Dias, F. B., Durack, P. J., Griffies, S. M., Harada, Y., Ilicak, M., Josey, S. A., Kobayashi, C., Kobayashi, S., Komuro, Y., Large, W. G., Sommer, J. L., Marsland, S. J., Masina, S., Scheinert, M., Tomita, H., Valdivieso, M., and Yamazaki, D.: JRA-55 based surface dataset for driving ocean–sea-ice models (JRA55-do), *Ocean Model.*, 130, 79–139, <https://doi.org/10.1016/j.ocemod.2018.07.002>, 2018.

- Turpin, B. J. and Lim, H.-J.: Species Contributions to PM<sub>2.5</sub> Mass Concentrations: Revisiting Common Assumptions for Estimating Organic Mass, *Aerosol Sci. Tech.*, 35, 602–610, <https://doi.org/10.1080/02786820152051454>, 2001.
- van Pinxteren, M., Zeppenfeld, S., Fomba, K. W., Triesch, N., Frka, S., and Herrmann, H.: Amino acids, carbohydrates, and lipids in the tropical oligotrophic Atlantic Ocean: sea-to-air transfer and atmospheric in situ formation, *Atmos. Chem. Phys.*, 23, 6571–6590, <https://doi.org/10.5194/acp-23-6571-2023>, 2023.
- Vergara-Temprado, J., Murray, B. J., Wilson, T. W., O’Sullivan, D., Browse, J., Pringle, K. J., Ardon-Dryer, K., Bertram, A. K., Burrows, S. M., Ceburnis, D., DeMott, P. J., Mason, R. H., O’Dowd, C. D., Rinaldi, M., and Carslaw, K. S.: Contribution of feldspar and marine organic aerosols to global ice nucleating particle concentrations, *Atmos. Chem. Phys.*, 17, 3637–3658, <https://doi.org/10.5194/acp-17-3637-2017>, 2017.
- Vergara-Temprado, J., Miltenberger, A. K., Furtado, K., Grosvenor, D. P., Shipway, B. J., Hill, A. A., Wilkinson, J. M., Field, P. R., Murray, B. J., and Carslaw, K. S.: Strong control of Southern Ocean cloud reflectivity by ice-nucleating particles, *P. Natl. Acad. Sci. USA*, 115, 2687–2692, <https://doi.org/10.1073/pnas.1721627115>, 2018.
- Vignati, E., Wilson, J., and Stier, P.: M7: An efficient size-resolved aerosol microphysics module for large-scale aerosol transport models, *J. Geophys. Res.-Atmos.*, 109, D22202, <https://doi.org/10.1029/2003JD004485>, 2004.
- Vignati, E., Facchini, M., Rinaldi, M., Scannell, C., Ceburnis, D., Sciare, J., Kanakidou, M., Myriokefalitakis, S., Dentener, F., and O’Dowd, C.: Global scale emission and distribution of sea-spray aerosol: Sea-salt and organic enrichment, *Atmos. Environ.*, 44, 670–677, <https://doi.org/10.1016/j.atmosenv.2009.11.013>, 2010.
- Wakeham, S. G., Lee, C., Hedges, J. I., Hernes, P. J., and Peterson, M. J.: Molecular indicators of diagenetic status in marine organic matter, *Geochim. Cosmochim. Ac.*, 61, 5363–5369, [https://doi.org/10.1016/S0016-7037\(97\)00312-8](https://doi.org/10.1016/S0016-7037(97)00312-8), 1997.
- Wang, Q., Danilov, S., Sidorenko, D., Timmermann, R., Wekerle, C., Wang, X., Jung, T., and Schröter, J.: The Finite Element Sea Ice-Ocean Model (FESOM) v.1.4: formulation of an ocean general circulation model, *Geosci. Model Dev.*, 7, 663–693, <https://doi.org/10.5194/gmd-7-663-2014>, 2014.
- Wang, Q., Wekerle, C., Danilov, S., Wang, X., and Jung, T.: A 4.5 km resolution Arctic Ocean simulation with the global multi-resolution model FESOM 1.4, *Geosci. Model Dev.*, 11, 1229–1255, <https://doi.org/10.5194/gmd-11-1229-2018>, 2018.
- Wekerle, C., Wang, Q., Danilov, S., Schourup-Kristensen, V., von Appen, W.-J., and Jung, T.: Atlantic Water in the Nordic Seas: Locally eddy-permitting ocean simulation in a global setup, *J. Geophys. Res.-Oceans*, 122, 914–940, <https://doi.org/10.1002/2016JC012121>, 2017.
- Wetz, M. S. and Wheeler, P. A.: Release of dissolved organic matter by coastal diatoms, *Limnol. Oceanogr.*, 52, 798–807, <https://doi.org/10.4319/lo.2007.52.2.0798>, 2007.
- Wilson, T. W., Ladino, L. A., Alpert, P. A., Breckels, M. N., Brooks, I. M., Browse, J., Burrows, S. M., Carslaw, K. S., Huffman, J. A., Judd, C., Kilsthau, W. P., Mason, R. H., McFiggans, G., Miller, L. A., Najera, J. J., Polishchuk, E., Rae, S., Schiller, C. L., Si, M., Temprado, J. V., Whale, T. F., Wong, J. P., Wurl, O., Yakobi-Hancock, J. D., Abbatt, J. P., Aller, J. Y., Bertram, A. K., Knopf, D. A., and Murray, B. J.: A marine biogenic source of atmospheric ice-nucleating particles, *Nature*, 525, 234–238, <https://doi.org/10.1038/nature14986>, 2015.
- Wolter, K.: Bacterial incorporation of organic substances released by natural phytoplankton populations., *Mar. Ecol. Prog. Ser.*, 7, 287–295, 1982.
- Yongmanitchai, W. and Ward, O. P.: Positional distribution of fatty acids, and molecular species of polar lipids, in the diatom *Phaeodactylum tricornutum*, *J. Gen. Microbiol.*, 139, 465–472, <https://doi.org/10.1099/00221287-139-3-465>, 1993.
- Yun, Y. and Penner, J. E.: An evaluation of the potential radiative forcing and climatic impact of marine organic aerosols as heterogeneous ice nuclei, *Geophys. Res. Lett.*, 40, 4121–4126, <https://doi.org/10.1002/grl.50794>, 2013.
- Zeising, M., Oziel, L., Gurses, O., Hauck, J., Losa, S., Silke, T., and Bracher, A.: Model code implementing TEP in FESOM2.1-REcoM3, Zenodo [code], <https://doi.org/10.5281/zenodo.14017537>, 2024.
- Zeppenfeld, S., van Pinxteren, M., Engel, A., and Herrmann, H.: A protocol for quantifying mono- and polysaccharides in seawater and related saline matrices by electro-dialysis (ED) – combined with HPAEC-PAD, *Ocean Sci.*, 16, 817–830, <https://doi.org/10.5194/os-16-817-2020>, 2020.
- Zeppenfeld, S., Pinxteren, M. V., Pinxteren, D. V., Wex, H., Berdalet, E., Vaqué, D., Dall’osto, M., and Herrmann, H.: Aerosol Marine Primary Carbohydrates and Atmospheric Transformation in the Western Antarctic Peninsula, *ACS Earth and Space Chemistry*, 5, 1032–1047, <https://doi.org/10.1021/acsearthspacechem.0c00351>, 2021.
- Zeppenfeld, S., van Pinxteren, M., Hartmann, M., Zeising, M., Bracher, A., and Herrmann, H.: Marine carbohydrates in Arctic aerosol particles and fog – diversity of oceanic sources and atmospheric transformations, *Atmos. Chem. Phys.*, 23, 15561–15587, <https://doi.org/10.5194/acp-23-15561-2023>, 2023.
- Zhao, X., Liu, X., Burrows, S. M., and Shi, Y.: Effects of marine organic aerosols as sources of immersion-mode ice-nucleating particles on high-latitude mixed-phase clouds, *Atmos. Chem. Phys.*, 21, 2305–2327, <https://doi.org/10.5194/acp-21-2305-2021>, 2021.